Numerische
Mathematik

A structure-preserving parametric finite element method for geometric flows with anisotropic surface energy

Weizhu Bao[1] · Yifei Li[1]

© The Author(s), under exclusive licence to Springer-Verlag GmbH Germany, part of Springer Nature 2024

Abstract

We propose and analyze a structure-preserving parametric finite element method (SP-PFEM) for the evolution of a closed curve under different geometric flows with arbitrary anisotropic surface energy density $\gamma(\boldsymbol{n})$, where $\boldsymbol{n} \in \mathbb{S}^1$ represents the outward unit normal vector. We begin with the anisotropic surface diffusion which possesses two well-known geometric structures—area conservation and energy dissipation—during the evolution of the closed curve. By introducing a novel surface energy matrix $\boldsymbol{G}_k(\boldsymbol{n})$ depending on $\gamma(\boldsymbol{n})$ and the Cahn-Hoffman $\boldsymbol{\xi}$-vector as well as a nonnegative stabilizing function $k(\boldsymbol{n})$, we obtain a new conservative geometric partial differential equation and its corresponding variational formulation for the anisotropic surface diffusion. Based on the new weak formulation, we propose a full discretization by adopting the parametric finite element method for spatial discretization and a semi-implicit temporal discretization with a proper and clever approximation for the outward normal vector. Under a mild and natural condition on $\gamma(\boldsymbol{n})$, we can prove that the proposed full discretization is structure-preserving, i.e. it preserves the area conservation and energy dissipation at the discretized level, and thus it is unconditionally energy stable. The proposed SP-PFEM is then extended to simulate the evolution of a close curve under other anisotropic geometric flows including anisotropic curvature flow and area-conserved anisotropic curvature flow. Extensive numerical results are reported to demonstrate the efficiency and unconditional energy stability as well as good mesh quality (and thus no need to re-mesh during the evolution) of the proposed SP-PFEM for simulating anisotropic geometric flows.

✉ Yifei Li
  e0444158@u.nus.edu

  Weizhu Bao
  matbaowz@nus.edu.sg
  https://blog.nus.edu.sg/matbwz/

[1] Department of Mathematics, National University of Singapore, Singapore 119076, Singapore

1 Introduction

Anisotropic surface energy along surface/interface is ubiquitous in solids and materials science due to the lattice orientational difference [16, 29]. It thus generates anisotropic evolution process of interface/surface (or geometric flows with anisotropic surface energy) in materials science [31, 41, 44], imaging science [19, 22, 37], and computational geometry [16, 20, 45]. In fact, anisotropic geometric flows have significant and broader applications in materials science, solid-state physics and computational geometry, such as grain boundary growth [13], foam bubble/film [40], surface phase formation [49], epitaxial growth [27, 29], heterogeneous catalysis [39], solid-state dewetting [5, 7, 44], and computational graphics [19, 22, 37].

Assume Γ be a closed curve in two dimensions (2D) associated with a given anisotropic surface energy density $\gamma(\boldsymbol{n})$, where $\boldsymbol{n} = (n_1, n_2)^T \in \mathbb{S}^1$ represents the outward unit normal vector, see Fig. 1. Define its corresponding free energy functional $W(\Gamma)$ as [4, 6, 20, 33, 42]:

$$W(\Gamma) := \int_{\Gamma} \gamma(\boldsymbol{n})ds, \tag{1.1}$$

where s denotes the arc-length parameter of Γ. By applying the thermodynamic variation, one can obtain the chemical potential $\mu := \mu(s)$ (or weighted curvature denoted as $\kappa_\gamma := \kappa_\gamma(s)$) generated from the energy functional $W(\Gamma)$ as [33, 42]

$$\mu = \kappa_\gamma := \frac{\delta W(\Gamma)}{\delta \Gamma} = \lim_{\varepsilon \to 0} \frac{W(\Gamma^\varepsilon) - W(\Gamma)}{\varepsilon}, \tag{1.2}$$

where Γ^ε is a small perturbation of Γ [33]. Different geometric flows associate with the anisotropic surface energy density $\gamma(\boldsymbol{n})$ can be easily defined by providing the nor-
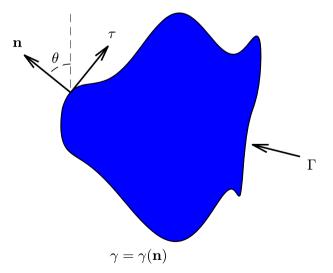

Fig. 1 An illustration of a closed curve Γ in 2D with an anisotropic surface energy density $\gamma(\boldsymbol{n})$ depending on the outward unit normal vector $\boldsymbol{n}$

mal velocity V_n for the evolution of Γ, which is usually generated from the chemical potential μ [15, 43]. Typical anisotropic geometric flows are widely used in different applications including anisotropic curvature flow, area-conserved anisotropic curvature flow and anisotropic surface diffusion with the corresponding normal velocity V_n given as [1, 14, 15, 18, 43]

$$V_n = \begin{cases} -\mu, & \text{anisotropic curvature flow,} \\ -\mu + \lambda, & \text{area-conserved anisotropic curvature flow,} \\ \partial_{ss}\mu, & \text{anisotropic surface diffusion,} \end{cases} \quad (1.3)$$

where the Lagrange multiplier λ is chosen such that the area of the region enclosed by Γ is conserved, which is given as

$$\lambda = \frac{\int_\Gamma \mu \, ds}{\int_\Gamma 1 \, ds} \quad \Leftrightarrow \quad \int_\Gamma V_n \, ds = \int_\Gamma (-\mu + \lambda) ds = 0. \quad (1.4)$$

We remark here that if $\gamma(\boldsymbol{n}) \equiv 1$ for $\boldsymbol{n} \in \mathbb{S}^1$, i.e. in the case of the isotropic surface energy density, the chemical potential μ defined in (1.2) collapses to the curvature κ of Γ. Then the geometric flows defined in (1.3) collapse to curvature flow (or curve-shortening flow), area-conserved curvature flow and surface diffusion, respectively [14].

For the geometric flows (1.3) with the isotropic surface energy density, i.e. $\gamma(\boldsymbol{n}) \equiv 1$ for $\boldsymbol{n} \in \mathbb{S}^1$, based on different parametrizations of Γ and different mathematical formulations for the flows, many different numerical methods have been proposed in the literature. These numerical methods include the level set method and the phase-field method [24], the marker particle method [23, 47], the finite element method based on graph formulation [20, 21], the discontinuous Galerkin method [48], the crystalline method [17, 28], the evolving surface finite element method (ESFEM) [34], and the parametric finite element method (PFEM) [9, 11, 20, 25, 26]. Among these numerical methods, most of them need to frequently carry out remeshing during the evolution in order to avoid the collision of mesh points, given that only the normal velocity is provided in the geometric flows (1.3). Therefore, different artificial tangential velocities are introduced in different numerical methods. One notable exception is the energy-stable PFEM (ES-PFEM) proposed by Barrett, Garcke, and Nürnberg (also called as BGN scheme in the literature). It demonstrates several good properties including efficiency, accuracy and unconditional energy stability as well as the surprising asymptotic equal-mesh distribution property for isotropic geometric flows [9, 11]. Recently, by introducing a clever approximation of the normal vector via an average of the two normal vectors at two adjacent time steps, Bao and Zhao proposed a structure-preserving PFEM (SP-PFEM) [2, 3, 8] for the isotropic surface diffusion. The SP-PFEM preserves the two geometric structures—mass (or the area of the region enclosed by the curve) conservation and energy (or the length of the curve) dissipation—in the fully discretized level.

Different techniques have been presented to extend the ES-PFEM and/or SP-PFEM from isotropic geometric flows to anisotropic geometric flows in the literature [10, 12, 32, 33, 35, 45]. When $\gamma(\boldsymbol{n})$ is taken as the Riemannian-like metric anisotropic surface

energy, by adapting a modified variational formulation with a proper and clever surface energy matrix, Barrett, Garcke and Nürnberg [10] extended successfully the ES-PFEM to anisotropic surface diffusion with this very special surface energy density. Recently, by introducing conservative geometric partial differential equations for the anisotropic surface diffusion with a general form of $\gamma(\boldsymbol{n}) = \gamma(-\sin\theta, \cos\theta) := \hat{\gamma}(\theta)$ with θ being the angle between $\boldsymbol{n}$ and the vertical axis (cf. Fig 1), we extended the ES-PFEM to the anisotropic surface diffusion under a very strong condition on $\hat{\gamma}(\theta)$ [35]. Very recently, by introducing a symmetric positive definite surface matrix $\boldsymbol{Z}_k(\boldsymbol{n})$ depending on $\gamma(\boldsymbol{n})$ and the Cahn-Hoffman $\boldsymbol{\xi}$-vector as well as a stabilizing function $k(\boldsymbol{n})$: $\mathbb{S}^1 \to \mathbb{R}^+$ [4, 6], we successfully and systematically extended the ES-PFEM and SP-PFEM methods from isotropic surface diffusion to anisotropic surface diffusion in two ($d = 2$) and three dimensions ($d = 3$) under a symmetric condition on $\gamma(\boldsymbol{n})$ as:

$$\gamma(-\boldsymbol{n}) = \gamma(\boldsymbol{n}), \qquad \boldsymbol{n} \in \mathbb{S}^{d-1}, \qquad \text{with} \quad d = 2, 3. \qquad (1.5)$$

To our best knowledge, it is still an open question to extend systematically either ES-PFEM or SP-PFEM for solving the anisotropic surface diffusion with arbitrary form of $\gamma(\boldsymbol{n})$, especially when $\gamma(\boldsymbol{n})$ is NOT symmetric, such as for the 3-fold anisotropic surface energy density arising in solid-state dewetting [5, 45].

The main objective of this paper is to extend the SP-PFEM (and ES-PFEM) for solving the anisotropic geometric flow (1.3) with the surface energy density $\gamma(\boldsymbol{n})$ satisfying a relatively mild and simple condition as

$$\gamma(-\boldsymbol{n}) < 3\gamma(\boldsymbol{n}), \quad \boldsymbol{n} \in \mathbb{S}^1, \qquad \gamma(\boldsymbol{p}) \in C^2(\mathbb{R}^2 \setminus \{\boldsymbol{0}\}), \qquad (1.6)$$

where $\gamma(\boldsymbol{p})$ is a one-homogeneous extension of $\gamma(\boldsymbol{n})$ from $\mathbb{S}^1$ to $\mathbb{R}^2$ defined as [4, 6]

$$\gamma(\boldsymbol{p}) := \begin{cases} |\boldsymbol{p}|\, \gamma\left(\frac{\boldsymbol{p}}{|\boldsymbol{p}|}\right), & \forall \boldsymbol{p} = (p_1, p_2)^T \in \mathbb{R}^2_* := \mathbb{R}^2 \setminus \{\boldsymbol{0}\}, \\ 0, & \boldsymbol{p} = \boldsymbol{0}, \end{cases} \qquad (1.7)$$

where $|\boldsymbol{p}| = \sqrt{p_1^2 + p_2^2}$. In fact, if $\gamma(\boldsymbol{n})$ is symmetric, i.e. it satisfies (1.5), then it satisfies (1.6) automatically since $0 < \gamma(-\boldsymbol{n}) = \gamma(\boldsymbol{n}) < 3\gamma(\boldsymbol{n})$ for $\boldsymbol{n} \in \mathbb{S}^1$, and thus the SP-PFEM proposed in this paper works for both symmetric and non-symmetric surface energy density $\gamma(\boldsymbol{n})$. The main ingredients in the proposed method are based on: (i) the introduction of a novel surface energy matrix $\boldsymbol{G}_k(\boldsymbol{n})$ depending on $\gamma(\boldsymbol{n})$ and the Cahn-Hoffman $\boldsymbol{\xi}$-vector as well as a stabilizing function $k(\boldsymbol{n})$: $\mathbb{S}^1 \to \mathbb{R}^+$, which can be explicitly decoupled into a symmetric positive definite matrix and an anti-symmetric matrix; (ii) a new conservative geometric partial differential equation (PDE) for the anisotropic geometric flows (1.3); (iii) a new variational formulation; and (iv) a proper approximation of the normal vector. Under the mild and simple condition (1.6) on the anisotropic surface energy density $\gamma(\boldsymbol{n})$, we can prove rigorously that the proposed SP-PFEM is structure-preserving—area conservation and energy dissipation—for the anisotropic surface diffusion in the discretized level. Then the proposed SP-PFEM is extended to simulate the evolution of a closed curve under other

anisotropic geometric flows including anisotropic curvature flow and area-conserved anisotropic curvature flow.

The remainder of this paper is organized as follows: In Sect. 2, by introducing the surface energy matrix $\boldsymbol{G}_k(\boldsymbol{n})$, we derive a new conservative PDE and its corresponding variational formulation for the anisotropic surface diffusion, and propose the semi-discretization in space and the full-discretization by SP-PFEM. In Sect. 3, we establish the unconditional energy dissipation of the proposed SP-PFEM for the anisotropic surface diffusion under the condition (1.6). In Sect. 4, we extend the proposed SP-PFEM to the anisotropic curvature flow and area-conserved anisotropic curvature flow. Extensive numerical results are reported in Sect. 5 to illustrate the efficiency and accuracy as well as structure-preserving properties of the proposed SP-PFEM. Finally, some concluding remarks are drawn in Sect. 6.

2 The structure-preserving PFEM for anisotropic surface diffusion

In this section, by taking the anisotropic surface diffusion in (1.3), we introduce a surface energy matrix $\boldsymbol{G}_k(\boldsymbol{n})$, obtain a conservative geometric PDE and derive its corresponding variational formulation. An SP-PFEM for the variational problem is presented and its structure-preserving property is stated under the simple and mild condition (1.6) on the anisotropic surface energy density $\gamma(\boldsymbol{n})$.

2.1 The geometric PDE

Let $\Gamma := \Gamma(t)$ be parameterized by $\boldsymbol{X} := \boldsymbol{X}(s, t) = (x(s, t), y(s, t))^T \in \mathbb{R}^2$ with s denoting the time-dependent arc-length parametrization (or 'Lagrangian coordinate') of Γ and t representing the time. Then the anisotropic surface diffusion of Γ can be described by

$$\partial_t \boldsymbol{X} = (\partial_{ss}\mu)\,\boldsymbol{n}, \tag{2.1}$$

where $\boldsymbol{n} = (n_1, n_2)^T \in \mathbb{S}^1$ represents the outward unit normal vector of Γ, and μ is the chemical potential given in (1.2). In practice, another popular way (or 'Eulerian coordinate') is to adopt $\rho \in \mathbb{T} = \mathbb{R}/\mathbb{Z} = [0, 1]$ being the periodic interval and then parameterize $\Gamma(t)$ on $\mathbb{T}$ by $\boldsymbol{X}(\rho, t)$, which is given as

$$\Gamma(t) := \boldsymbol{X}(\mathbb{T}, t) \quad \boldsymbol{X}(\cdot, t) : \mathbb{T} \to \mathbb{R}^2, (\rho, t) \mapsto (x(\rho, t), y(\rho, t))^T. \tag{2.2}$$

Then the arc-length parameter s is given as $s(\rho, t) = \int_0^\rho |\partial_\rho \boldsymbol{X}(\rho, t)|\, d\rho$ satisfying $\partial_\rho s = |\partial_\rho \boldsymbol{X}|$. We assume that the parametrization by ρ is regular during the evolution, i.e., there is a constant $C > 1$ such that $\frac{1}{C} \leq |\partial_\rho s(\rho, t)| \leq C$. The normal velocity V_n can be given by this parametrization as

$$V_n = \boldsymbol{n} \cdot \partial_t \boldsymbol{X}. \tag{2.3}$$

Based on the one-homogeneous extension $\gamma(\boldsymbol{p})$ in (1.7), we can talk about the regularity of $\gamma(\boldsymbol{n})$ by referring to the regularity of $\gamma(\boldsymbol{p})$, i.e., $\gamma(\boldsymbol{n}) \in C^2(\mathbb{S}^1) \iff$

$\gamma(\boldsymbol{p}) \in C^2(\mathbb{R}^2 \backslash \{\boldsymbol{0}\})$. The Cahn-Hoffman $\boldsymbol{\xi}$-vector is widely adopted in the literature as [30, 46]

$$\boldsymbol{\xi} := \boldsymbol{\xi}(\boldsymbol{n}) : \mathbb{S}^1 \to \mathbb{R}^2, \quad \boldsymbol{n} \mapsto \boldsymbol{\xi}(\boldsymbol{n}) = (\xi_1, \xi_2)^T := \nabla \gamma(\boldsymbol{p})|_{\boldsymbol{p}=\boldsymbol{n}} = \gamma(\boldsymbol{n})\boldsymbol{n} + (\boldsymbol{\xi} \cdot \boldsymbol{\tau})\boldsymbol{\tau}, \tag{2.4}$$

here $\boldsymbol{\tau} = \partial_s X = \boldsymbol{n}^\perp$ is the unit tangential vector of Γ, and $\perp$ denotes the clockwise rotation by $\frac{\pi}{2}$. Then an explicit formulation of the chemical potential μ in (1.2) can be expressed in term of the $\boldsymbol{\xi}$-vector as [33]

$$\mu := \mu(\boldsymbol{n}) = -\boldsymbol{n} \cdot \partial_s \boldsymbol{\xi}^\perp. \tag{2.5}$$

Thus another equivalent geometric PDE for the anisotropic surface diffusion can be written as

$$\boldsymbol{n} \cdot \partial_t X = \partial_{ss} \mu, \tag{2.6a}$$

$$\mu = -\boldsymbol{n} \cdot \partial_s \boldsymbol{\xi}^\perp, \qquad \boldsymbol{\xi}(\boldsymbol{n}) = \nabla \gamma(\boldsymbol{p})|_{\boldsymbol{p}=\boldsymbol{n}}. \tag{2.6b}$$

2.2 The surface energy matrix

Introduce the surface energy matrix $\boldsymbol{G}_k(\boldsymbol{n})$ as

$$\boldsymbol{G}_k(\boldsymbol{n}) := \gamma(\boldsymbol{n})I_2 - \boldsymbol{n}\boldsymbol{\xi}^T + \boldsymbol{\xi}\boldsymbol{n}^T + k(\boldsymbol{n})\boldsymbol{n}\boldsymbol{n}^T := \boldsymbol{G}_k^{(s)}(\boldsymbol{n}) + \boldsymbol{G}^{(a)}(\boldsymbol{n}), \quad \forall \boldsymbol{n} \in \mathbb{S}^1, \tag{2.7}$$

where I_2 is the 2×2 identity matrix, $k(\boldsymbol{n}) : \mathbb{S}^1 \to \mathbb{R}^+$ is a nonnegative stabilizing function to be determined later, and $\boldsymbol{G}_k^{(s)}(\boldsymbol{n})$ and $\boldsymbol{G}^{(a)}(\boldsymbol{n})$ are a symmetric positive matrix and an anti-symmetric matrix, respectively, which are given as

$$\boldsymbol{G}_k^{(s)}(\boldsymbol{n}) := \gamma(\boldsymbol{n})I_2 + k(\boldsymbol{n})\boldsymbol{n}\boldsymbol{n}^T, \quad \boldsymbol{G}^{(a)}(\boldsymbol{n}) := -\boldsymbol{n}\boldsymbol{\xi}^T + \boldsymbol{\xi}\boldsymbol{n}^T, \quad \forall \boldsymbol{n} \in \mathbb{S}^1. \tag{2.8}$$

Then we get the following relationship between the weighted curvature μ and the newly constructed $\boldsymbol{G}_k(\boldsymbol{n})$.

Lemma 2.1 *The weighted curvature μ defined in (2.5) has the following alternative explicit expression*

$$\mu \boldsymbol{n} = -\partial_s(\boldsymbol{G}_k(\boldsymbol{n})\partial_s X). \tag{2.9}$$

Proof From [4, Lemma 2.1], we know that $\boldsymbol{\xi}$ and μ given in (2.4) and (2.5), respectively, satisfy

$$\mu \boldsymbol{n} = -\partial_s \boldsymbol{\xi}^\perp, \quad \boldsymbol{\xi}^\perp = \gamma(\boldsymbol{n})\boldsymbol{\tau} - (\boldsymbol{\xi} \cdot \boldsymbol{\tau})\boldsymbol{n}. \tag{2.10}$$

Thus it suffices to show $\boldsymbol{G}_k(\boldsymbol{n})\partial_s X = \boldsymbol{\xi}^\perp$. Since $\partial_s X = \boldsymbol{\tau}$, by using the definition of $\boldsymbol{G}_k(\boldsymbol{n})$ in (2.7), we can simplify $\boldsymbol{G}_k(\boldsymbol{n})\partial_s X$ as

$$\boldsymbol{G}_k(\boldsymbol{n})\partial_s X = \gamma(\boldsymbol{n})\boldsymbol{\tau} - (\boldsymbol{\xi} \cdot \boldsymbol{\tau})\boldsymbol{n} + (\boldsymbol{n} \cdot \boldsymbol{\tau})\boldsymbol{\xi} + k(\boldsymbol{n})(\boldsymbol{n} \cdot \boldsymbol{\tau})\boldsymbol{n}$$
$$= \gamma(\boldsymbol{n})\boldsymbol{\tau} - (\boldsymbol{\xi} \cdot \boldsymbol{\tau})\boldsymbol{n} = \boldsymbol{\xi}^\perp. \tag{2.11}$$

Combining this with (2.10), we get the desired equality (2.9).   □

By applying (2.9), the geometric PDE for the anisotropic surface diffusion (2.6) can be rewritten as the following *conservative form*

$$\boldsymbol{n} \cdot \partial_t \boldsymbol{X} = \partial_{ss} \mu, \tag{2.12a}$$

$$\mu \boldsymbol{n} = -\partial_s (\boldsymbol{G}_k(\boldsymbol{n}) \partial_s \boldsymbol{X}). \tag{2.12b}$$

Here the 'conservative form' refers to the right-hand side of (2.12b) is in conservative form with respect to s.

Remark 2.1 When $\gamma(\boldsymbol{n}) \equiv 1$ for $\boldsymbol{n} \in \mathbb{S}^1$, i.e., isotropic case, it is well known that $\boldsymbol{\xi} = \boldsymbol{n}$. Taking $k(\boldsymbol{n}) \equiv 0$ for $\boldsymbol{n} \in \mathbb{S}^1$ in (2.7), we get $\boldsymbol{G}_k(\boldsymbol{n}) = I_2$. Then the conservative form (2.9) (and (2.12)) collapses to the standard forms used in the literature for the isotropic case [9]. Thus our new formulation (2.9) (and (2.12)) is a natural extension from the isotropic case to anisotropic case.

On the other hand, when $\gamma(\boldsymbol{n}) \neq 1$, i.e., anisotropic case, it is well known that $\boldsymbol{0} \neq \boldsymbol{\xi} \neq \boldsymbol{n}$, and then $-\boldsymbol{n}\boldsymbol{\xi}^T + \boldsymbol{\xi}\boldsymbol{n}^T \neq -\boldsymbol{n}\boldsymbol{\xi}^T - \boldsymbol{\xi}\boldsymbol{n}^T$ since $\boldsymbol{\xi}\boldsymbol{n}^T \neq \boldsymbol{0}$. Thus our new surface energy matrix $\boldsymbol{G}_k(\boldsymbol{n})$ introduced in (2.7) is quite different with the surface energy matrix $\boldsymbol{Z}_k(\boldsymbol{n})$ introduced in [4, 6] mainly for anisotropic case with symmetric surface energy density $\gamma(-\boldsymbol{n}) = \gamma(\boldsymbol{n})$.

Remark 2.2 As it is illustrated in Fig. 1, we have

$$\begin{aligned}
\boldsymbol{n} &= (n_1, n_2)^T = (-\sin\theta, \cos\theta)^T := \boldsymbol{n}(\theta), \\
\boldsymbol{\tau} &= (\tau_1, \tau_2)^T = (\cos\theta, \sin\theta)^T := \boldsymbol{\tau}(\theta), \qquad \theta \in [-\pi, \pi], \\
\gamma(\boldsymbol{n}) &= \gamma(-\sin\theta, \cos\theta) := \hat{\gamma}(\theta).
\end{aligned} \tag{2.13}$$

Plugging (1.7) into (2.4) and taking $\boldsymbol{p} = |\boldsymbol{p}|(-\sin\theta, \cos\theta)^T$, we get

$$\begin{aligned}
\boldsymbol{\xi} = \boldsymbol{\xi}(\boldsymbol{n}) = \nabla\gamma(\boldsymbol{p})|_{\boldsymbol{p}=\boldsymbol{n}} &= \left[\gamma\left(\frac{\boldsymbol{p}}{|\boldsymbol{p}|}\right) \nabla|\boldsymbol{p}| + |\boldsymbol{p}|\nabla\gamma\left(\frac{\boldsymbol{p}}{|\boldsymbol{p}|}\right) \right]\Bigg|_{\boldsymbol{p}=\boldsymbol{n}} \\
&= \gamma(-\sin\theta, \cos\theta)\boldsymbol{n}(\theta) + \nabla\gamma(-\sin\theta, \cos\theta) \\
&= \hat{\gamma}(\theta)\boldsymbol{n}(\theta) - \hat{\gamma}'(\theta)\boldsymbol{\tau}(\theta) := \hat{\boldsymbol{\xi}}(\theta).
\end{aligned} \tag{2.14}$$

Substituting (2.14) into (2.7), we have

$$\boldsymbol{G}_k(\boldsymbol{n}) = \begin{pmatrix} \hat{\gamma}(\theta) & -\hat{\gamma}'(\theta) \\ \hat{\gamma}'(\theta) & \hat{\gamma}(\theta) \end{pmatrix} + \hat{k}(\theta) \begin{pmatrix} \sin^2\theta & -\sin\theta\cos\theta \\ -\sin\theta\cos\theta & \cos^2\theta \end{pmatrix} := \hat{\boldsymbol{G}}_k(\theta), \tag{2.15}$$

where $\hat{k}(\theta) := k(\boldsymbol{n}) = k(-\sin\theta, \cos\theta)$ is a stabilizing function. If we take $\hat{k}(\theta) \equiv 0$ in (2.15), then $\hat{\boldsymbol{G}}_k(\theta)$ collapses to the surface energy matrix $G(\theta)$ proposed in [35]. Thus our formulation is also a natural extension of the method in [35] which adopts the surface energy density in $\hat{\gamma}(\theta)$ formulation and thus cannot be extended to three dimensions (3D). On the contrary, since we adopt the surface energy density in the

$\gamma(\boldsymbol{n})$ formulation, our method can be extended to 3D straightforwardly via the Cahn-Hoffman $\boldsymbol{\xi}$-vector.

Moreover, due to the stabilizing function $k(\boldsymbol{n}) = \hat{k}(\theta)$, the energy stable condition (1.6) becomes

$$\hat{\gamma}(\theta + \pi) < 3\hat{\gamma}(\theta), \quad \forall \theta \in [-\pi, \pi], \qquad \hat{\gamma}(\theta) \in C^2([-\pi, \pi]). \tag{2.16}$$

This energy stable condition significantly improve the conditions required in [35] without using the stabilizing function, i.e., $\hat{k}(\theta) \equiv 0$. For example, for the m-fold anisotropic surface energy density $\hat{\gamma}(\theta) = 1 + \beta \cos m\theta$ for $m = 2, 3, 4, 6$: the energy stable condition in [35] (without using the stabilizing function $\hat{k}(\theta)$) requires $|\beta| \leq \frac{1}{m^2+1}$ for all m; while it only needs $|\beta| < 1$ and $|\beta| < \frac{1}{2}$ for m being even and odd, respectively. Thus by introducing the stabilizing function $k(\boldsymbol{n})$ (or $\hat{k}(\theta)$), we can improve the energy stable condition significantly.

2.3 A variational formulation and its properties

We then derive the variational formulation for the conservative form (2.12). Suppose the usual L^2 space over $\mathbb{T}$ is

$$L^2(\mathbb{T}) := \left\{ u : \mathbb{T} \to \mathbb{R} \mid \int_{\mathbb{T}} |u(\rho)|^2 d\rho < \infty \right\}. \tag{2.17}$$

The functional space with respect to $\Gamma := \Gamma(t)$ can be given as

$$L^2(\Gamma(t)) := \left\{ u : \mathbb{T} \to \mathbb{R} \mid \int_{\mathbb{T}} |u(\rho)|^2 \partial_\rho s(\rho, t) d\rho < \infty \right\}, \tag{2.18}$$

with the following weighted L^2-inner product $(\cdot, \cdot)_{\Gamma(t)}$

$$\left(u, v \right)_{\Gamma(t)} := \int_{\Gamma(t)} u(s)v(s)ds = \int_{\mathbb{T}} u(\rho)v(\rho)\partial_\rho s(\rho, t) \, d\rho, \quad \forall u, v \in L^2(\mathbb{T}). \tag{2.19}$$

Since we assume that the parameterization is regular; the space $L^2(\Gamma(t))$ with respect to $\Gamma(t)$ is equivalent to the usual $L^2(\mathbb{T})$, which is independent of t. The Sobolev space $H^1(\mathbb{T})$ is defined as

$$H^1(\mathbb{T}) := \left\{ u : \mathbb{T} \to \mathbb{R} \mid u \in L^2(\mathbb{T}), \partial_s u \in L^2(\mathbb{T}) \right\}. \tag{2.20}$$

Here $\partial_s u$ is the weak derivative. Moreover, we can extend the above definitions to the functions in $[L^2(\mathbb{T})]^2$ and $[H^1(\mathbb{T})]^2$.

Multiplying a test function $\phi \in H^1(\mathbb{T})$ to (2.12a), integrating over $\Gamma(t)$ and taking integration by parts, we obtain

$$\left(\boldsymbol{n} \cdot \partial_t \boldsymbol{X}, \phi \right)_{\Gamma(t)} = -\left(\partial_s \mu, \partial_s \phi \right)_{\Gamma(t)}. \tag{2.21}$$

Similarly, by multiplying a test function $\boldsymbol{\omega} = (\omega_1, \omega_2)^T \in [H^1(\mathbb{T})]^2$ to (2.12b), we deduce that

$$\left(\mu\boldsymbol{n}, \boldsymbol{\omega}\right)_{\Gamma(t)} = \left(\boldsymbol{G}_k(\boldsymbol{n})\partial_s X, \partial_s \boldsymbol{\omega}\right)_{\Gamma(t)}. \tag{2.22}$$

Based on the two Eqs. (2.21) and (2.22), the new variational formulation for the conservative form (2.12) can be stated as follows: Suppose the initial curve $\Gamma_0 := X(\cdot, 0) = (x(\cdot, 0), y(\cdot, 0))^T \in [H^1(\mathbb{T})]^2$ and the initial weighted curvature $\mu(\cdot, 0) := \mu_0(\cdot) \in H^1(\mathbb{T})$, then for any $t > 0$, find the solution $(X(\cdot, t), \mu(\cdot, t)) \in [H^1(\mathbb{T})]^2 \times H^1(\mathbb{T})$ satisfying

$$\left(\boldsymbol{n} \cdot \partial_t X, \varphi\right)_{\Gamma(t)} + \left(\partial_s \mu, \partial_s \varphi\right)_{\Gamma(t)} = 0, \qquad \forall \varphi \in H^1(\mathbb{T}), \tag{2.23a}$$

$$\left(\mu\boldsymbol{n}, \boldsymbol{\omega}\right)_{\Gamma(t)} - \left(\boldsymbol{G}_k(\boldsymbol{n})\partial_s X, \partial_s \boldsymbol{\omega}\right)_{\Gamma(t)} = 0, \quad \forall \boldsymbol{\omega} \in [H^1(\mathbb{T})]^2. \tag{2.23b}$$

Denote the area of the region enclosed by $\Gamma(t)$ as $A(t)$ and the free interfacial energy of $\Gamma(t)$ as $W(t)$, which are given by

$$A(t) := \int_{\Gamma(t)} y(\rho, t)\partial_\rho x(\rho, t)d\rho, \quad W(t) := \int_{\Gamma(t)} \gamma(\boldsymbol{n})\,ds, \qquad t \geq 0. \tag{2.24}$$

We can show that the two geometric properties, i.e. area conservation and energy dissipation, still hold for the weak formulation (2.23).

Proposition 2.1 *(area conservation and energy dissipation) Suppose $\Gamma(t)$ is given by the solution $(X(\cdot, t), \mu(\cdot, t))$ of the variational formulation (2.23), we have*

$$A(t) \equiv A(0), \qquad W(t) \leq W(t_1) \leq W(0), \qquad \forall t \geq t_1 \geq 0. \tag{2.25}$$

Proof By taking $\varphi = 1$ in (2.23a) and using (2.17) in [35], we know

$$\frac{dA(t)}{dt} = \left(\partial_t X, \boldsymbol{n}\right)_{\Gamma(t)} = -\left(\partial_s \mu, \partial_s 1\right)_{\Gamma(t)} = 0.$$

Therefore we have $A(t) \equiv A(0)$, $\forall t \geq 0$. For the energy dissipation, from the proof of [4, Proposition 2.2], it holds

$$\frac{dW(t)}{dt} = \left(\gamma(\boldsymbol{n})\partial_s X - (\boldsymbol{\xi} \cdot \partial_s X)\boldsymbol{n}, \partial_s \partial_t X\right)_{\Gamma(t)}. \tag{2.26}$$

By setting $\varphi = \mu$ in (2.23a) and $\boldsymbol{\omega} = \partial_t X$ in (2.23b), and considering (2.11) and (2.26), we deduce that

$$\frac{dW(t)}{dt} = \left(\boldsymbol{G}_k(\boldsymbol{n})\partial_s X, \partial_s \partial_t X\right)_{\Gamma(t)} = \left(\mu\boldsymbol{n}, \partial_t X\right)_{\Gamma(t)} = -\tau\left(\partial_s \mu, \partial_s \mu\right)_{\Gamma(t)} \leq 0.$$

Which indicates the energy dissipation $W(t) \leq W(t_1) \leq W(0)$, $\forall t \geq t_1 \geq 0$. □

2.4 A semi-discretization in space

To obtain the spatial discretization, let $N > 2$ be an integer and define the mesh size as $h = \frac{1}{N}$. Consider the uniform partition of $\mathbb{T} = [0, 1] = \cup_{j=1}^{N} I_j$, where $I_j = [\rho_{j-1}, \rho_j]$ and $\rho_j = jh$ for $j = 0, 1, \ldots, N$. Here $\rho_N = \rho_0$ by periodicity. The closed curve $\Gamma(t) = X(\cdot, t)$ is approximated by the closed line segments $\Gamma^h(t) = X^h(\cdot, t) = (x^h(\cdot, t), y^h(\cdot, t))^T$ satisfying $X^h(\rho_j, 0) = X(\rho_j, 0)$. And the discretization for the test function space $H^1(\mathbb{T})$ is given by the following space of piecewise linear finite element functions

$$\mathbb{K}^h = \mathbb{K}^h(\mathbb{T}) := \left\{ u \in C(\mathbb{T}) | \ u|_{I_j} \in \mathcal{P}^1(I_j), \forall 1 \leq j \leq N \right\}, \tag{2.27}$$

where $\mathcal{P}^1(I_j)$ is the set of polynomials defined on I_j of degree ≤ 1. The mass lumped inner product for two functions $u, v \in \mathbb{K}^h(\mathbb{T})$ with respect to $\Gamma^h(t)$ is defined as

$$(u, v)_{\Gamma^h(t)}^h := \frac{1}{2} \sum_{j=1}^{N} |\boldsymbol{h}_j(t)| \left((u \cdot v)(\rho_{j-1}^+) + (u \cdot v)(\rho_j^-) \right). \tag{2.28}$$

where $\boldsymbol{h}_j(t) = X^h(\rho_j, t) - X^h(\rho_{j-1}, t)$, and $u(\rho_j^{\pm}) = \lim_{\rho \to \rho_j^{\pm}} u(\rho)$. We note this mass lumped inner product is also applicable for $[\mathbb{K}^h]^2$ and the piecewise constant vector-valued functions with possible jump discontinuities at ρ_j for $0 \leq j \leq N$.

The discretized unit normal vector $\boldsymbol{n}^h(t)$, unit tangential vector $\boldsymbol{\tau}^h(t)$, and the $\boldsymbol{\xi}$-vector $\boldsymbol{\xi}^h(t)$ are such piecewise constant vectors on $\Gamma^h(t)$, which are given as

$$\boldsymbol{n}_j^h := \boldsymbol{n}^h|_{I_j} = -\frac{\boldsymbol{h}_j^{\perp}}{|\boldsymbol{h}_j|}, \quad \boldsymbol{\tau}_j^h := \boldsymbol{\tau}^h|_{I_j} = (\boldsymbol{n}_j^h)^{\perp}, \quad \boldsymbol{\xi}_j^h := \boldsymbol{\xi}^h|_{I_j} = \nabla \gamma(\boldsymbol{p})|_{\boldsymbol{p}=\boldsymbol{n}_j^h}. \tag{2.29}$$

Here we use $\boldsymbol{n}^h$ to represent $\boldsymbol{n}^h(t)$ for short. To make sure $\boldsymbol{n}^h, \boldsymbol{\tau}^h, \boldsymbol{\xi}^h$ are well defined, we need the following assumption on $\boldsymbol{h}_j(t)$

$$\min_{1 \leq j \leq N} |\boldsymbol{h}_j(t)| > 0, \quad \forall t \geq 0. \tag{2.30}$$

After giving all the continuous objects their discretized versions, we can state the spatial semi-discretization as follows: Let $\Gamma_0^h := X^h(\mathbb{T}, 0) \in [\mathbb{K}^h]^2$, $\mu^h(\cdot, 0) \in \mathbb{K}^h$ be the approximations of $\Gamma_0 := X_0(\mathbb{T})$, $\mu_0(\cdot)$, respectively, with $X^h(\rho_j, 0) = X(\rho_j, 0)$, $\mu^h(\rho_j, 0) = \mu_0(\rho_j)$ for $0 \leq j \leq N$, find the solution $(X^h(\cdot, t), \mu^h(\cdot, t)) \in [\mathbb{K}^h]^2 \times \mathbb{K}^h$, such that

$$\left(\boldsymbol{n}^h \cdot \partial_t X^h, \varphi^h \right)_{\Gamma^h(t)}^h + \left(\partial_s \mu^h, \partial_s \varphi^h \right)_{\Gamma^h(t)}^h = 0, \qquad \forall \varphi^h \in \mathbb{K}^h, \tag{2.31a}$$

$$\left(\mu^h \boldsymbol{n}^h, \boldsymbol{\omega}^h \right)_{\Gamma^h(t)}^h - \left(G_k(\boldsymbol{n}^h) \partial_s X^h, \partial_s \boldsymbol{\omega}^h \right)_{\Gamma^h(t)}^h = 0, \qquad \forall \boldsymbol{\omega}^h \in [\mathbb{K}^h]^2, \tag{2.31b}$$

where

$$\boldsymbol{G}_k(\boldsymbol{n}^h)|_{I_j} = \gamma(\boldsymbol{n}_j^h)I_2 - \boldsymbol{n}_j^h(\boldsymbol{\xi}_j^h)^T + \boldsymbol{\xi}_j^h(\boldsymbol{n}_j^h)^T + k(\boldsymbol{n}_j^h)\,\boldsymbol{n}_j^h(\boldsymbol{n}_j^h)^T, \qquad (2.32)$$

and the discretized derivative ∂_s for a scalar and vector valued functions f and $\boldsymbol{f}$, respectively, are given as

$$\partial_s f|_{I_j} := \frac{f(\rho_j) - f(\rho_{j-1})}{|\boldsymbol{h}_j|}, \quad \partial_s \boldsymbol{f}|_{I_j} := \frac{\boldsymbol{f}(\rho_j) - \boldsymbol{f}(\rho_{j-1})}{|\boldsymbol{h}_j|}, \qquad (2.33)$$

and assumption (2.30) ensures $\partial_s f$ and $\partial_s \boldsymbol{f}$ are piecewise constant functions with possible jump discontinuities at ρ_j for $0 \le j \le N$, thus the mass lumped inner product terms like $\left(\partial_s \mu^h, \partial_s \varphi^h\right)_{\Gamma^h(t)}^h$ in (2.31) are well defined.

Denote the enclosed area and the total energy of the closed line segments $\Gamma^h(t)$ as $A^h(t)$ and $W^h(t)$, respectively, which are given by

$$A^h(t) = \frac{1}{2}\sum_{j=1}^{N}(x_j^h(t) - x_{j-1}^h(t))(y_j^h(t) + y_{j-1}^h(t)), \quad W^h(t) = \sum_{j=1}^{N}|\boldsymbol{h}_j(t)|\gamma(\boldsymbol{n}_j^h), \tag{2.34}$$

where $x_j^h(t) := x^h(\rho_j, t), y_j^h(t) := y^h(\rho_j, t), \forall 0 \le j \le N$.

Given that the finite element space $\mathbb{K}^h$ is the subspace of $H^1(\mathbb{T})$, the spatial semi-discretization (2.31) is a conforming discretization. Therefore, the structure-preserving property (2.25) of the weak formulation still holds for (2.31).

Proposition 2.2 *(Area conservation and energy dissipation) Suppose $\Gamma^h(t)$ is given by the solution $(\boldsymbol{X}^h(\cdot, t), \mu^h(\cdot, t))$ of (2.31), then we have*

$$A^h(t) \equiv A^h(0), \quad W^h(t) \le W^h(t_1) \le W^h(0), \quad \forall t \ge t_1 \ge 0. \tag{2.35}$$

The proof is similar to [35, Proposition 3.1], and is omitted for brevity.

2.5 A structure-preserving PFEM

We then consider the full discretization. Let τ be the uniform time step, and $\Gamma^m = \boldsymbol{X}^m(\mathbb{T}) \in [\mathbb{K}^h]^2$ be the approximation of $\Gamma^h(t_m) = \boldsymbol{X}^h(\mathbb{T}, t_m), \forall m \ge 0$, where $t_m := m\tau$. Suppose $\boldsymbol{h}_j^m := \boldsymbol{X}^m(\rho_j) - \boldsymbol{X}^m(\rho_{j-1})$, we can similarly give the definitions for the mass lumped inner product $(\cdot, \cdot)_{\Gamma^m}^h$ as well as the unit normal vector $\boldsymbol{n}^m$, the unit tangential vector $\boldsymbol{\tau}^m$, and the $\boldsymbol{\xi}$-vector $\boldsymbol{\xi}^m$ with respect to Γ^m. By adopting the backward semi-implicit Euler method, the fully-implicit structure-preserving discretization of PFEM for anisotropic surface diffusion (2.6) can then be given as:

Suppose the initial approximation $\Gamma^0 = \boldsymbol{X}^0(\mathbb{T}) \in [\mathbb{K}^h]^2$ is given by $\boldsymbol{X}^0(\rho_j) = \boldsymbol{X}_0(\rho_j), \forall 0 \le j \le N$. For any $m = 0, 1, 2, \ldots$, find the solution

$(\boldsymbol{X}^m(\cdot) = (x^m(\cdot), y^m(\cdot))^T, \mu^m(\cdot)) \in [\mathbb{K}^h]^2 \times \mathbb{K}^h$, such that

$$\left(\boldsymbol{n}^{m+\frac{1}{2}} \cdot \frac{\boldsymbol{X}^{m+1} - \boldsymbol{X}^m}{\tau}, \varphi^h\right)_{\Gamma^m}^h + \left(\partial_s \mu^{m+1}, \partial_s \varphi^h\right)_{\Gamma^m}^h = 0, \quad \forall \varphi^h \in \mathbb{K}^h, \qquad (2.36a)$$

$$\left(\mu^{m+1} \boldsymbol{n}^{m+\frac{1}{2}}, \boldsymbol{\omega}^h\right)_{\Gamma^m}^h - \left(\boldsymbol{G}_k(\boldsymbol{n}^m)\partial_s \boldsymbol{X}^{m+1}, \partial_s \boldsymbol{\omega}^h\right)_{\Gamma^m}^h = 0, \quad \forall \boldsymbol{\omega}^h \in [\mathbb{K}^h]^2, \quad (2.36b)$$

where

$$\boldsymbol{G}_k(\boldsymbol{n}^m)|_{I_j} = \gamma(\boldsymbol{n}_j^m)I_2 - \boldsymbol{n}_j^m(\boldsymbol{\xi}_j^m)^T + \boldsymbol{\xi}_j^m(\boldsymbol{n}_j^m)^T + k(\boldsymbol{n}_j^m)\,\boldsymbol{n}_j^m(\boldsymbol{n}_j^m)^T, \qquad (2.37)$$

and

$$\boldsymbol{n}^{m+\frac{1}{2}} := -\frac{1}{2}\frac{1}{|\partial_\rho \boldsymbol{X}^m|}(\partial_\rho \boldsymbol{X}^m + \partial_\rho \boldsymbol{X}^{m+1})^\perp. \qquad (2.38)$$

The SP-PFEM (2.36) is fully-implicit, and can be numerically solved by Newton's iterative method. Here we adapt the iterative solver, originally proposed for isotropic surface diffusion in [8], to solve our SP-PFEM (2.36) of anisotropic surface diffusion. The only change is we replace their identity matrix I_2 with our surface energy matrix $\boldsymbol{G}_k(\boldsymbol{n}^m)$. We observe that most variables, especially the integral domain Γ^m, are treated explicitly, the non-linearity arises from $\boldsymbol{n}^{m+\frac{1}{2}}$. If $\boldsymbol{n}^{m+\frac{1}{2}}$ is replaced by $\boldsymbol{n}^m$, then (2.36) becomes semi-implicit. However, the clever approximation $\boldsymbol{n}^{m+\frac{1}{2}}$ is critical in preserving the area conservation, and the semi-implicit PFEM can only preserve the energy dissipation property.

2.6 Main results

Denote the enclosed area and the total energy of the closed line segments Γ^m as A^m and W^m, respectively, which are given by

$$A^m = \frac{1}{2}\sum_{j=1}^N (x^m(\rho_j) - x^m(\rho_{j-1}))(y^m(\rho_j) + y^m(\rho_{j-1})), \qquad (2.39a)$$

$$W^m = \sum_{j=1}^N |\boldsymbol{h}_j^m|\gamma(\boldsymbol{n}_j^m). \qquad (2.39b)$$

Introduce two auxiliary functions $P_\alpha(\boldsymbol{n}, \hat{\boldsymbol{n}}), Q(\boldsymbol{n}, \hat{\boldsymbol{n}})$ as

$$P_\alpha(\boldsymbol{n}, \hat{\boldsymbol{n}}) := 2\sqrt{(\gamma(\boldsymbol{n}) + \alpha(\hat{\boldsymbol{n}} \cdot \boldsymbol{n}^\perp)^2)\gamma(\boldsymbol{n})}, \quad \forall \boldsymbol{n} \in \mathbb{S}^1, \quad \alpha \geq 0, \qquad (2.40a)$$

$$Q(\boldsymbol{n}, \hat{\boldsymbol{n}}) := \gamma(\hat{\boldsymbol{n}}) + \gamma(\boldsymbol{n})(\boldsymbol{n} \cdot \hat{\boldsymbol{n}}) - (\boldsymbol{\xi} \cdot \boldsymbol{n}^\perp)(\hat{\boldsymbol{n}} \cdot \boldsymbol{n}^\perp), \quad \forall \boldsymbol{n}, \hat{\boldsymbol{n}} \in \mathbb{S}^1, \qquad (2.40b)$$

we define the minimal stabilizing function $k_0(\boldsymbol{n})$ as (its existence will be given in the next section)

$$k_0(\boldsymbol{n}) := \inf\{\alpha \geq 0 : P_\alpha(\boldsymbol{n}, \hat{\boldsymbol{n}}) - Q(\boldsymbol{n}, \hat{\boldsymbol{n}}) \geq 0, \; \forall \hat{\boldsymbol{n}} \in \mathbb{S}^1\}, \quad \forall \boldsymbol{n} \in \mathbb{S}^1. \qquad (2.41)$$

For the SP-PFEM (2.36), we have

Theorem 2.1 *(Structure-preserving) Under the simple and mild condition (1.6) on the anisotropic surface energy $\gamma(\boldsymbol{n})$ and taking the stabilizing function $k(\boldsymbol{n}) \geq k_0(\boldsymbol{n})$ for $\boldsymbol{n} \in \mathbb{S}^1$, then the SP-PFEM (2.36) preserves the two geometric properties—mass conservation and energy dissipation—in the discrete level, i.e.,*

$$A^{m+1} \equiv A^0, \qquad W^{m+1} \leq W^m \leq \ldots \leq W^0, \qquad \forall m \geq 0. \qquad (2.42)$$

The area conservation part is a direct result of [8, Theorem 2.1]. And the energy dissipation will be proved in the next section.

Remark 2.3 The construction of the two auxiliary functions $P_\alpha(\boldsymbol{n}, \hat{\boldsymbol{n}})$, $Q(\boldsymbol{n}, \hat{\boldsymbol{n}})$ are inspired by [35]. Indeed, as elaborated in Remark 2.1, [35] is a special case $\alpha = 0$ of this paper, and its energy stability result was established by showing that $Q(\boldsymbol{n}, \hat{\boldsymbol{n}}) - 2\gamma(\boldsymbol{n}) \leq 0 = P_0(\boldsymbol{n}, \hat{\boldsymbol{n}}) - 2\gamma(\boldsymbol{n})$.

3 Energy dissipation of the SP-PFEM (2.36)

In this section, we first show if $\gamma(\boldsymbol{n})$ satisfies (1.6), the minimal stabilizing function $k_0(\boldsymbol{n})$ defined in (2.41) is well-defined, thus we can always choose a nonnegative stabilizing function $k(\boldsymbol{n}) \geq k_0(\boldsymbol{n})$ for $\boldsymbol{n} \in \mathbb{S}^1$. After that, we will use $k_0(\boldsymbol{n})$ to give the proof of the unconditional energy stability part of the main theorem 2.1.

3.1 Existence of the minimal stabilizing function $k_0(n)$ defined in (2.41)

From the definition of $k_0(\boldsymbol{n})$ in (2.41), we observe that if $(\hat{\boldsymbol{n}} \cdot \boldsymbol{n}^\perp)^2 > 0$, then intuitively for sufficiently large α, we know the $P_\alpha(\boldsymbol{n}, \hat{\boldsymbol{n}}) \geq Q(\boldsymbol{n}, \hat{\boldsymbol{n}})$. But this approach will fail when $(\hat{\boldsymbol{n}} \cdot \boldsymbol{n}^\perp)^2 = 0$, and this can happen if $\hat{\boldsymbol{n}} = \pm\boldsymbol{n}$, which suggests us to treat the two cases $\hat{\boldsymbol{n}} \cdot \boldsymbol{n} \geq 0$ and $\hat{\boldsymbol{n}} \cdot \boldsymbol{n} \leq 0$ separately. To simplify the notations, we introduce a compact set $\mathbb{S}_{\boldsymbol{n}}^1$ as

$$\mathbb{S}_{\boldsymbol{n}}^1 := \{\hat{\boldsymbol{n}} \in \mathbb{S}^1 | \boldsymbol{n} \cdot \hat{\boldsymbol{n}} \geq 0\}, \quad \boldsymbol{n} \in \mathbb{S}^1. \qquad (3.1)$$

Then $\boldsymbol{n} \cdot \hat{\boldsymbol{n}} \geq 0 \iff \hat{\boldsymbol{n}} \in \mathbb{S}_{\boldsymbol{n}}^1$, and $\boldsymbol{n} \cdot \hat{\boldsymbol{n}} \leq 0 \iff \hat{\boldsymbol{n}} \in \mathbb{S}_{-\boldsymbol{n}}^1$.

Theorem 3.1 *The $k_0(\boldsymbol{n})$ defined as (2.41) is bounded if the condition (1.6) on $\gamma(\boldsymbol{n})$ is satisfied.*

Proof First we consider the case $\hat{\boldsymbol{n}} \in \mathbb{S}_{\boldsymbol{n}}^1$. Since $\gamma(\boldsymbol{n})$ satisfies (1.6), we know $\gamma(\boldsymbol{p}) \in C^2(\mathbb{R}^2 \backslash \{\boldsymbol{0}\})$. Thus there exists a constant $C_1 > 0$, such that

$$\left\| \mathbf{H}_\gamma(\boldsymbol{p}) \right\|_2 \leq C_1, \quad \forall \frac{1}{2} \leq |\boldsymbol{p}|^2 \leq 1, \qquad (3.2)$$

here $\mathbf{H}_\gamma$ is the Hessian matrix of $\gamma(\boldsymbol{p})$, and $\|\cdot\|_2$ denotes the 2-norm.

By mean value theorem, we know for all $\hat{\boldsymbol{n}} \in \mathbb{S}_n^1$, there exists a constant $0 < c < 1$ such that

$$\gamma(\hat{\boldsymbol{n}}) = \gamma(\boldsymbol{n}) + \boldsymbol{\xi} \cdot (\hat{\boldsymbol{n}} - \boldsymbol{n}) + \frac{1}{2}(\hat{\boldsymbol{n}} - \boldsymbol{n})^T \mathbf{H}_\gamma \left(c\boldsymbol{n} + (1 - c)\hat{\boldsymbol{n}}\right)(\hat{\boldsymbol{n}} - \boldsymbol{n}). \quad (3.3)$$

It is easy to see that $|c\boldsymbol{n} + (1 - c)\hat{\boldsymbol{n}}| \leq 1$ and $|c\boldsymbol{n} + (1 - c)\hat{\boldsymbol{n}}|^2 \geq c^2 + (1 - c)^2 \geq \frac{1}{2}$. Hence we know

$$\gamma(\hat{\boldsymbol{n}}) \leq \gamma(\boldsymbol{n}) + \boldsymbol{\xi} \cdot (\hat{\boldsymbol{n}} - \boldsymbol{n}) + \frac{C_1}{2}|\hat{\boldsymbol{n}} - \boldsymbol{n}|^2. \quad (3.4)$$

And notice that $\boldsymbol{\xi} \cdot \boldsymbol{n} = \gamma(\boldsymbol{n})$, we can then get the following estimate of $Q(\boldsymbol{n}, \hat{\boldsymbol{n}})$:

$$\begin{aligned} Q(\boldsymbol{n}, \hat{\boldsymbol{n}}) &- 2\gamma(\boldsymbol{n}) \\ &\leq \left(\gamma(\boldsymbol{n}) + \boldsymbol{\xi} \cdot (\hat{\boldsymbol{n}} - \boldsymbol{n}) + \frac{C_1}{2}|\hat{\boldsymbol{n}} - \boldsymbol{n}|^2\right) - \left(\boldsymbol{\xi} \cdot \hat{\boldsymbol{n}} - (\boldsymbol{\xi} \cdot \boldsymbol{n})(\hat{\boldsymbol{n}} \cdot \boldsymbol{n})\right) \\ &\quad + \gamma(\boldsymbol{n})(\boldsymbol{n} \cdot \hat{\boldsymbol{n}}) - 2\gamma(\boldsymbol{n}) \\ &= 2\gamma(\boldsymbol{n})((\boldsymbol{n} \cdot \hat{\boldsymbol{n}}) - 1) + \frac{C_1}{2}|\hat{\boldsymbol{n}} - \boldsymbol{n}|^2 \\ &= \left(\frac{C_1}{2} - \gamma(\boldsymbol{n})\right)|\hat{\boldsymbol{n}} - \boldsymbol{n}|^2. \end{aligned} \quad (3.5)$$

Here we use the fact $\boldsymbol{\xi} \cdot \hat{\boldsymbol{n}} = (\boldsymbol{\xi} \cdot \boldsymbol{n})(\hat{\boldsymbol{n}} \cdot \boldsymbol{n}) + (\boldsymbol{\xi} \cdot \boldsymbol{n}^\perp)(\hat{\boldsymbol{n}} \cdot \boldsymbol{n}^\perp)$ and $|\hat{\boldsymbol{n}} - \boldsymbol{n}|^2 = 2 - 2\boldsymbol{n} \cdot \hat{\boldsymbol{n}}$.

On the other hand, using the fact $(\hat{\boldsymbol{n}} \cdot \boldsymbol{n}^\perp)^2 = 1 - (\hat{\boldsymbol{n}} \cdot \boldsymbol{n})^2 = \frac{|\hat{\boldsymbol{n}}-\boldsymbol{n}|^2}{2}(1 + \boldsymbol{n} \cdot \hat{\boldsymbol{n}})$, we know that for $\alpha > \gamma(\boldsymbol{n})$, it holds

$$\begin{aligned} P_\alpha(\boldsymbol{n}, \hat{\boldsymbol{n}}) - 2\gamma(\boldsymbol{n}) &= \frac{2\alpha(\hat{\boldsymbol{n}} \cdot \boldsymbol{n}^\perp)^2}{\sqrt{1 + \frac{\alpha}{\gamma(\boldsymbol{n})}(\hat{\boldsymbol{n}} \cdot \boldsymbol{n}^\perp)^2} + 1} \\ &\geq \frac{2\alpha(\hat{\boldsymbol{n}} \cdot \boldsymbol{n}^\perp)^2}{2\sqrt{1 + \frac{\alpha}{\gamma(\boldsymbol{n})}}} = \frac{\alpha(1 + \hat{\boldsymbol{n}} \cdot \boldsymbol{n})}{2\sqrt{1 + \frac{\alpha}{\gamma(\boldsymbol{n})}}}|\hat{\boldsymbol{n}} - \boldsymbol{n}|^2 \\ &\geq \frac{\sqrt{\gamma(\boldsymbol{n})(\alpha - \gamma(\boldsymbol{n}))}}{2}|\hat{\boldsymbol{n}} - \boldsymbol{n}|^2. \end{aligned} \quad (3.6)$$

Combining (3.5) and (3.6), we know that for $\alpha \geq \alpha_1 := \frac{(C_1 - 2\gamma(\boldsymbol{n}))^2 + \gamma^2(\boldsymbol{n})}{\gamma(\boldsymbol{n})} < \infty$, it holds $P_\alpha(\boldsymbol{n}, \hat{\boldsymbol{n}}) \geq Q(\boldsymbol{n}, \hat{\boldsymbol{n}}), \forall \hat{\boldsymbol{n}} \in \mathbb{S}_n^1$.

For the case $\hat{\boldsymbol{n}} \in \mathbb{S}_{-n}^1$, by (1.6), when $\hat{\boldsymbol{n}} = -\boldsymbol{n}$, we know that

$$\begin{aligned} Q(\boldsymbol{n}, -\boldsymbol{n}) &= \gamma(-\boldsymbol{n}) + \gamma(\boldsymbol{n})(\boldsymbol{n} \cdot (-\boldsymbol{n})) - (\boldsymbol{\xi} \cdot \boldsymbol{n}^\perp)(-\boldsymbol{n} \cdot \boldsymbol{n}^\perp) \\ &< 3\gamma(\boldsymbol{n}) - \gamma(\boldsymbol{n}) = 2\gamma(\boldsymbol{n}). \end{aligned} \quad (3.7)$$

Thus for $\alpha = 0 := \alpha_{-n} < \infty$, we know $P_0(\boldsymbol{n}, -\boldsymbol{n}) = 2\gamma(\boldsymbol{n}) > Q(\boldsymbol{n}, -\boldsymbol{n})$. By continuity of P_α and Q, there exits an open set $\mathcal{O}_{-n,0} \subset \mathbb{S}^1$ such that $-\boldsymbol{n} \in \mathcal{O}_{-n,0}$,

and for all $\hat{\boldsymbol{n}} \in \mathcal{O}_{-\boldsymbol{n},0}$ and $\alpha \geq 0$, we have $P_\alpha(\boldsymbol{n}, \hat{\boldsymbol{n}}) - Q(\boldsymbol{n}, \hat{\boldsymbol{n}}) \geq 0$. For a given $\boldsymbol{p} \in \mathbb{S}^1_{-\boldsymbol{n}}$, $\boldsymbol{p} \neq -\boldsymbol{n}$, we know that $(\boldsymbol{p} \cdot \boldsymbol{n}^\perp)^2 > 0$. Therefore we can choose a sufficiently large but finite $\alpha_{\boldsymbol{p}} < \infty$, such that $P_{\alpha_{\boldsymbol{p}}}(\boldsymbol{n}, \boldsymbol{p}) - Q(\boldsymbol{n}, \boldsymbol{p}) > 0$. And by the same argument, there exists an open set $\mathcal{O}_{\boldsymbol{p},\alpha_{\boldsymbol{p}}} \subset \mathbb{S}^1$, such that $\boldsymbol{p} \in \mathcal{O}_{\boldsymbol{p},\alpha_{\boldsymbol{p}}}$ and $P_\alpha(\boldsymbol{n}, \hat{\boldsymbol{n}}) - Q(\boldsymbol{n}, \hat{\boldsymbol{n}}) \geq 0, \forall \hat{\boldsymbol{n}} \in \mathcal{O}_{\boldsymbol{p},\alpha_{\boldsymbol{p}}}, \alpha \geq \alpha_{\boldsymbol{p}}$. And we obtain an open cover for $\mathbb{S}^1_{-\boldsymbol{n}}$ as

$$\mathbb{S}^1_{-\boldsymbol{n}} \subset \bigcup_{\boldsymbol{p} \in \mathbb{S}^1_{-\boldsymbol{n}}} \mathcal{O}_{\boldsymbol{p},\alpha_{\boldsymbol{p}}}. \tag{3.8}$$

Since $\mathbb{S}^1_{-\boldsymbol{n}}$ is compact, by open cover theorem, there is a finite set of vectors $\boldsymbol{p}_1, \ldots, \boldsymbol{p}_M \in \mathbb{S}^1_{-\boldsymbol{n}}$, such that

$$\mathbb{S}^1_{-\boldsymbol{n}} \subset \bigcup_{i=1}^{M} \mathcal{O}_{\boldsymbol{p}_i,\alpha_{\boldsymbol{p}_i}}. \tag{3.9}$$

If we take $\alpha_2 := \max_{1 \leq i \leq M} \alpha_{\boldsymbol{p}_i} < \infty$, we have $P_\alpha(\boldsymbol{n}, \hat{\boldsymbol{n}}) - Q(\boldsymbol{n}, \hat{\boldsymbol{n}}) \geq 0, \forall \hat{\boldsymbol{n}} \in \mathbb{S}^1_{-\boldsymbol{n}}, \alpha \geq \alpha_2$, hence

$$\infty > \max(\alpha_1, \alpha_2) \in \left\{ \alpha \geq 0 : P_\alpha(\boldsymbol{n}, \hat{\boldsymbol{n}}) - Q(\boldsymbol{n}, \hat{\boldsymbol{n}}) \geq 0, \ \forall \hat{\boldsymbol{n}} \in \mathbb{S}^1 \right\}. \tag{3.10}$$

Which means $k_0(\boldsymbol{n}) = \inf \left\{ \alpha \geq 0 : P_\alpha(\boldsymbol{n}, \hat{\boldsymbol{n}}) - Q(\boldsymbol{n}, \hat{\boldsymbol{n}}) \geq 0, \forall \hat{\boldsymbol{n}} \in \mathbb{S}^1 \right\} < \infty$. $\qquad \square$

Remark 3.1 The $\hat{\boldsymbol{n}} \in \mathbb{S}^1_{\boldsymbol{n}}$ part only requires inequality (3.4), thus condition $\gamma(\boldsymbol{p}) \in C^2(\mathbb{R}^2 \backslash \{\boldsymbol{0}\})$ can be relaxed to $\gamma(\boldsymbol{p})$ is piecewise $C^2(\mathbb{R}^2 \setminus \{\boldsymbol{0}\})$. And the condition $\gamma(-\boldsymbol{n}) < 3\gamma(\boldsymbol{n})$ is to ensure the existence of $\mathcal{O}_{-\boldsymbol{n},0}$, which suggests we may find a larger $\alpha_{-\boldsymbol{n}} > 0$ such that $\mathcal{O}_{-\boldsymbol{n},\alpha_{-\boldsymbol{n}}}$ exists for $\gamma(\boldsymbol{n})$ satisfies $\gamma(-\boldsymbol{n}) \leq 3\gamma(\boldsymbol{n})$. And by the same argument, we can show such $\mathcal{O}_{-\boldsymbol{n},\alpha_{-\boldsymbol{n}}}$ exists if and only if $\boldsymbol{\xi}(\boldsymbol{n}_i) = \gamma(\boldsymbol{n}_i)\boldsymbol{n}_i \iff \gamma(-\boldsymbol{n}_i) = 3\gamma(\boldsymbol{n}_i)$.

By the existence of $k_0(\boldsymbol{n})$, once the $\gamma(\boldsymbol{n})$ is given, the minimal stabilizing function $k_0(\boldsymbol{n})$ is then determined, i.e. there is a map from $\gamma(\boldsymbol{n})$ to $k_0(\boldsymbol{n})$. Similar to the proof when $\gamma(\boldsymbol{n})$ is symmetric, i.e. $\gamma(-\boldsymbol{n}) = \gamma(\boldsymbol{n})$ in [2, 8], we can show such map is a sub-linear with respect to $\gamma(\boldsymbol{n})$ when it satisfies (1.6).

Lemma 3.1 *(Positive homogeneity and subadditivity) Let $\gamma_1(\boldsymbol{n})$, $\gamma_2(\boldsymbol{n})$ and $\gamma_3(\boldsymbol{n})$ be three functions satisfying (1.6) with minimal stabilizing functions $k_0^{(1)}(\boldsymbol{n})$, $k_0^{(2)}(\boldsymbol{n})$ and $k_0^{(3)}(\boldsymbol{n})$, respectively, then we have*

(i) if $\gamma_2(\boldsymbol{n}) = c\gamma_1(\boldsymbol{n})$, where $c > 0$ is a positive number, then $k_0^{(2)}(\boldsymbol{n}) = ck_0^{(1)}(\boldsymbol{n})$; and

(ii) if $\gamma_3(\boldsymbol{n}) = \gamma_1(\boldsymbol{n}) + \gamma_2(\boldsymbol{n})$, then $k_0^{(3)}(\boldsymbol{n}) \leq k_0^{(1)}(\boldsymbol{n}) + k_0^{(2)}(\boldsymbol{n})$.

Proof Let $\boldsymbol{\xi}^{(i)}$, $P_\alpha^{(i)}(\boldsymbol{n}, \hat{\boldsymbol{n}})$, $Q^{(i)}(\boldsymbol{n}, \hat{\boldsymbol{n}})$, $k_0^{(i)}(\boldsymbol{n})$ be the $\boldsymbol{\xi}$-vector, the auxiliary function $P_\alpha(\boldsymbol{n}, \hat{\boldsymbol{n}})$, $Q(\boldsymbol{n}, \hat{\boldsymbol{n}})$ and the minimal stabilizing function $k_0(\boldsymbol{n})$ for $\gamma_i(\boldsymbol{n})$, $i = 1, 2, 3$, respectively.

(i) If $\gamma_2(\boldsymbol{n}) = c\gamma_1(\boldsymbol{n})$ with $c > 0$, then it is easy to see that

$$\boldsymbol{\xi}^{(2)} = c\,\boldsymbol{\xi}^{(1)}, \quad P_{c\alpha}^{(2)}(\boldsymbol{n}, \hat{\boldsymbol{n}}) = c\,P_\alpha^{(1)}(\boldsymbol{n}, \hat{\boldsymbol{n}}), \quad Q^{(2)}(\boldsymbol{n}, \hat{\boldsymbol{n}}) = c\,Q^{(1)}(\boldsymbol{n}, \hat{\boldsymbol{n}}).$$

This, together with the definition of $k_0^{(1)}(\boldsymbol{n})$ yields that

$$P_{c\,k_0^{(1)}(\boldsymbol{n})}^{(2)}(\boldsymbol{n}, \hat{\boldsymbol{n}}) - Q^{(2)}(\boldsymbol{n}, \hat{\boldsymbol{n}}) = c\left(P_{k_0^{(1)}(\boldsymbol{n})}^{(1)}(\boldsymbol{n}, \hat{\boldsymbol{n}}) - Q^{(1)}(\boldsymbol{n}, \hat{\boldsymbol{n}})\right) \geq 0.$$

Which indicates $k_0^{(2)}(\boldsymbol{n}) \leq c\,k_0^{(1)}(\boldsymbol{n})$. Similarly, $\gamma_1(\boldsymbol{n}) = \frac{1}{c}\gamma_2(\boldsymbol{n})$ implies that $k_0^{(1)}(\boldsymbol{n}) \leq \frac{1}{c}k_0^{(2)}(\boldsymbol{n})$. Therefore, we obtain $k_0^{(2)}(\boldsymbol{n}) = c\,k_0^{(1)}(\boldsymbol{n})$.

(ii) If $\gamma_3(\boldsymbol{n}) = \gamma_1(\boldsymbol{n}) + \gamma_2(\boldsymbol{n})$, then from (2.40b) it is easy to see $\boldsymbol{\xi}^{(3)} = \boldsymbol{\xi}^{(1)} + \boldsymbol{\xi}^{(2)}$ and $Q^{(3)}(\boldsymbol{n}, \hat{\boldsymbol{n}}) = Q^{(1)}(\boldsymbol{n}, \hat{\boldsymbol{n}}) + Q^{(2)}(\boldsymbol{n}, \hat{\boldsymbol{n}})$.

On the other hand, for any $a, b > 0$, by using the Cauchy inequality and noting (2.40a), we derive that

$$P_{a+b}^{(3)}(\boldsymbol{n}, \hat{\boldsymbol{n}})$$
$$= 2\sqrt{\left[\left(\gamma_1(\boldsymbol{n}) + a(\hat{\boldsymbol{n}} \cdot \boldsymbol{n}^\perp)^2\right) + \left(\gamma_2(\boldsymbol{n}) + b(\hat{\boldsymbol{n}} \cdot \boldsymbol{n}^\perp)^2\right)\right]\left[(\gamma_1(\boldsymbol{n})) + (\gamma_2(\boldsymbol{n}))\right]}$$
$$\geq 2\sqrt{\left(\sqrt{\left(\gamma_1(\boldsymbol{n}) + a(\hat{\boldsymbol{n}} \cdot \boldsymbol{n}^\perp)^2\right)\gamma_1(\boldsymbol{n})} + \sqrt{\left(\gamma_2(\boldsymbol{n}) + b(\hat{\boldsymbol{n}} \cdot \boldsymbol{n}^\perp)^2\right)\gamma_2(\boldsymbol{n})}\right)^2}$$
$$= P_a^{(1)}(\boldsymbol{n}, \hat{\boldsymbol{n}}) + P_b^{(2)}(\boldsymbol{n}, \hat{\boldsymbol{n}}). \tag{3.11}$$

Taking $a = k_0^{(1)}(\boldsymbol{n}) > 0$, $b = k_0^{(2)}(\boldsymbol{n}) > 0$ in (3.11) and using the definition of $k_0(\boldsymbol{n})$, we find that

$$P_{k_0^{(1)}(\boldsymbol{n})+k_0^{(2)}(\boldsymbol{n})}^{(3)}(\boldsymbol{n}, \hat{\boldsymbol{n}}) - Q^{(3)}(\boldsymbol{n}, \hat{\boldsymbol{n}})$$
$$\geq P_{k_0^{(1)}(\boldsymbol{n})}^{(1)}(\boldsymbol{n}, \hat{\boldsymbol{n}}) + P_{k_0^{(2)}(\boldsymbol{n})}^{(2)}(\boldsymbol{n}, \hat{\boldsymbol{n}}) - Q^{(1)}(\boldsymbol{n}, \hat{\boldsymbol{n}}) - Q^{(2)}(\boldsymbol{n}, \hat{\boldsymbol{n}}) \geq 0,$$

which indicates $k_0^{(3)}(\boldsymbol{n}) \leq k_0^{(1)}(\boldsymbol{n}) + k_0^{(2)}(\boldsymbol{n})$. $\qquad\square$

3.2 Proof of the energy dissipation in (2.42)

To prove the main result, we first need the following lemma:

Lemma 3.2 *Suppose* $\boldsymbol{h}, \hat{\boldsymbol{h}}$ *are two non-zero vectors in* $\mathbb{R}^2$ *and* $\boldsymbol{n} = -\frac{\boldsymbol{h}^\perp}{|\boldsymbol{h}|}$, $\hat{\boldsymbol{n}} = -\frac{\hat{\boldsymbol{h}}^\perp}{|\hat{\boldsymbol{h}}|}$ *to be the corresponding unit normal vectors. Then for any* $k(\boldsymbol{n}) \geq k_0(\boldsymbol{n})$*, the following inequality holds*

$$\frac{1}{|\boldsymbol{h}|}\left(G_k(\boldsymbol{n})\hat{\boldsymbol{h}}\right) \cdot (\hat{\boldsymbol{h}} - \boldsymbol{h}) \geq |\hat{\boldsymbol{h}}|\gamma(\hat{\boldsymbol{n}}) - |\boldsymbol{h}|\,\gamma(\boldsymbol{n}). \tag{3.12}$$

Proof By applying the definition of $G_k(n)$ in (2.7) and $P_\alpha(n, \hat{n})$ in (2.40a), and noticing $\hat{h} = \hat{n}^\perp |\hat{h}|$, $n \cdot \hat{n}^\perp = -\hat{n} \cdot n^\perp$, the term $\frac{1}{|h|} \left(G_k(n)\hat{h} \right) \cdot \hat{h}$ can be simplified as

$$\frac{1}{|h|} \left(G_k(n)\hat{h} \right) \cdot \hat{h}$$

$$= \frac{1}{|h|} \left[\left((\gamma(n)I_2 + k(n)n(n)^T) + (\xi(n)^T - n(\xi)^T) \right) \hat{h} \right] \cdot \hat{h}$$

$$= \frac{1}{|h|} \left[\left(\gamma(n)I_2 + k(n)n(n)^T \right) \hat{h} \right] \cdot \hat{h}$$

$$= \frac{1}{|h|} \left(\gamma(n)|\hat{h}|^2 + k(n)(n \cdot \hat{h})^2 \right)$$

$$= \frac{1}{|h|} \left(\gamma(n)|\hat{h}|^2 + k(n)(\hat{n} \cdot (n)^\perp)^2 |\hat{h}|^2 \right) = \frac{|\hat{h}|^2}{4|h|\gamma(n)} P^2_{k(n)}(n, \hat{n}). \qquad (3.13)$$

Similarly, by applying the definition of $G_k(n)$ in (2.7) and $Q(n, \hat{n})$ in (2.40b), and noticing $h = n^\perp |h|$, $\hat{h} = \hat{n}^\perp |\hat{h}|$, $h \cdot \hat{h} = n \cdot \hat{n}|h||\hat{h}|$, $n \cdot \hat{n}^\perp = -\hat{n} \cdot n^\perp$, the term $\frac{1}{|h|} \left(G_k(n)\hat{h} \right) \cdot h$ can be simplified as

$$\frac{1}{|h|} \left(G_k(n)\hat{h} \right) \cdot h = \frac{1}{|h|} \left(G_k^T(n)h \right) \cdot \hat{h}$$

$$= \frac{1}{|h|} \left[\left((\gamma(n)I_2 + n(\xi)^T) + (-\xi(n)^T + k(n)n(n)^T) \right) h \right] \cdot \hat{h}$$

$$= \frac{1}{|h|} \left[\left(\gamma(n)I_2 + n(\xi)^T \right) h \right] \cdot \hat{h}$$

$$= \frac{1}{|h|} \left[\gamma(n)(h \cdot \hat{h}) + (\xi \cdot h)(n \cdot \hat{h}) \right]$$

$$= |\hat{h}| \left(\gamma(n)(n \cdot \hat{n}) + (\xi \cdot n^\perp)(n \cdot \hat{n}^\perp) \right)$$

$$= |\hat{h}| \left(\gamma(n)(n \cdot \hat{n}) - (\xi \cdot n^\perp)(\hat{n} \cdot n^\perp) \right) = |\hat{h}| \left(Q(n, \hat{n}) - \gamma(\hat{n}) \right). \qquad (3.14)$$

Finally, combining the definition of $k_0(n)$ (2.41), (3.13), (3.14), and the fact $\frac{a^2}{4|h|\gamma(n)} \geq ab - |h|\gamma(n)b^2$ yields that

$$\frac{1}{|h|} \left(G_k(n)\hat{h} \right) \cdot (\hat{h} - h) = \frac{|\hat{h}|^2}{4|h|\gamma(n)} P^2_{k(n)}(n, \hat{n}) - |\hat{h}| \left(Q(n, \hat{n}) - \gamma(\hat{n}) \right)$$

$$\geq |\hat{h}|P_{k(n)} - |h|\gamma(n) - |\hat{h}| \left(P_{k(n)}(n, \hat{n}) - \gamma(\hat{n}) \right)$$

$$= |\hat{h}|\gamma(\hat{n}) - |h|\gamma(n), \qquad (3.15)$$

which validates (3.12). □

Now we can prove the energy dissipation part in our main result Theorem 2.1.

Proof The key point of the proof is to establish the following energy estimation

$$\left(G_k(\boldsymbol{n}^m)\partial_s \boldsymbol{X}^{m+1}, \partial_s(\boldsymbol{X}^{m+1} - \boldsymbol{X}^m) \right)_{\Gamma^m}^h \geq W^{m+1} - W^m, \quad m \geq 0. \tag{3.16}$$

For any $1 \leq j \leq N$, take $\boldsymbol{h} = \boldsymbol{h}_j^m$, $\hat{\boldsymbol{h}} = \boldsymbol{h}_j^{m+1}$ in Lemma 3.2, we know that $\boldsymbol{n} = -\frac{\boldsymbol{h}^\perp}{|\boldsymbol{h}|} = \boldsymbol{n}_j^m$, $\hat{\boldsymbol{n}} = \boldsymbol{n}_j^{m+1}$, and the following inequality holds

$$\frac{1}{|\boldsymbol{h}_j^m|} \left(G_k(\boldsymbol{n}_j^m)\boldsymbol{h}_j^{m+1} \right) \cdot (\boldsymbol{h}_j^{m+1} - \boldsymbol{h}_j^m) \geq |\boldsymbol{h}_j^{m+1}|\gamma(\boldsymbol{n}_j^{m+1}) - |\boldsymbol{h}_j^m|\gamma(\boldsymbol{n}_j^m). \tag{3.17}$$

Taking the summation over $1 \leq j \leq N$ for (3.17) and notice (2.28) and (2.39b), we have

$$\left(G_k(\boldsymbol{n}^m)\partial_s \boldsymbol{X}^{m+1}, \partial_s(\boldsymbol{X}^{m+1} - \boldsymbol{X}^m) \right)_{\Gamma^m}^h$$

$$= \sum_{j=1}^N \left[|\boldsymbol{h}_j^m| \left(G_k(\boldsymbol{n}_j^m)\frac{\boldsymbol{h}_j^{m+1}}{|\boldsymbol{h}_j^m|} \right) \cdot \frac{\boldsymbol{h}_j^{m+1} - \boldsymbol{h}_j^m}{|\boldsymbol{h}_j^m|} \right]$$

$$= \sum_{j=1}^N \left[\frac{1}{|\boldsymbol{h}_j^m|} \left(G_k(\boldsymbol{n}_j^m)\boldsymbol{h}_j^{m+1} \right) \cdot (\boldsymbol{h}_j^{m+1} - \boldsymbol{h}_j^m) \right]$$

$$\geq \sum_{j=1}^N \left[|\boldsymbol{h}_j^{m+1}|\gamma(\boldsymbol{n}_j^{m+1}) - |\boldsymbol{h}_j^m|\gamma(\boldsymbol{n}_j^m) \right]$$

$$= W^{m+1} - W^m, \quad \forall m = 0, 1, \dots$$

which proves the energy estimation in (3.16).

Finally, take $\varphi^h = \mu^{m+1}$ in (2.36a) and $\boldsymbol{\omega}^h = \boldsymbol{X}^{m+1} - \boldsymbol{X}^m$ in (2.36b), we have

$$0 \geq -\tau \left(\partial_s \mu^{m+1}, \partial_s \mu^{m+1} \right)_{\Gamma^m}^h$$

$$= \left(\boldsymbol{n}^{m+\frac{1}{2}} \cdot \left(\boldsymbol{X}^{m+1} - \boldsymbol{X}^m \right), \mu^{m+1} \right)_{\Gamma^m}^h$$

$$= \left(G_k(\boldsymbol{n}^m)\partial_s \boldsymbol{X}^{m+1}, \partial_s(\boldsymbol{X}^{m+1} - \boldsymbol{X}^m) \right)_{\Gamma^m}^h \geq W^{m+1} - W^m,$$

this is true for any m; therefore, the energy W^m decreases monotonically, and the proof is completed. $\qquad\square$

Remark 3.2 The condition $\gamma(\boldsymbol{p}) \in C^2(\mathbb{R}^2\backslash\{\boldsymbol{0}\})$ in (1.6) is natural, but $\gamma(-\boldsymbol{n}) < 3\gamma(\boldsymbol{n})$ looks quite complicated and seems not very sharp. However, the proof shows the condition $\gamma(-\boldsymbol{n}) < 3\gamma(\boldsymbol{n})$ is indeed natural! To see this, inequality (3.12) in Lemma 3.2 is essential in showing the energy estimate (3.16). And if we take $\hat{\boldsymbol{h}} = -\boldsymbol{h}$ in

Lemma 3.2, then $\hat{\boldsymbol{n}} = -\boldsymbol{n}$, and the inequality (3.12) becomes

$$2\gamma(\boldsymbol{n})\,|\boldsymbol{h}| \geq |\boldsymbol{h}|\,\gamma(-\boldsymbol{n}) - \gamma(\boldsymbol{n})\,|\boldsymbol{h}| \iff \gamma(-\boldsymbol{n})|\boldsymbol{h}| \leq 3\gamma(\boldsymbol{n})|\boldsymbol{h}|, \qquad (3.18)$$

which means $\gamma(-\boldsymbol{n}) \leq 3\gamma(\boldsymbol{n})$. Our sufficient condition for energy stability, as stated in (1.6), replaces $\geq$ with $>$, thus it is both natural and **almost necessary**.

4 Extension to other anisotropic geometric flows

In fact, the energy stable condition on $\gamma(\boldsymbol{n})$ in (1.6), the definition of $\boldsymbol{G}_k(\boldsymbol{n})$ in (2.7), the alternative expression for μ in (2.9), and the definition of $k_0(\boldsymbol{n})$ in (2.41) are independent of the anisotropic surface diffusion flow. Thus these definitions and even the proof of energy stability can be directly extended to other anisotropic geometric flows.

4.1 Anisotropic curvature flow

Similar to (2.12), for the anisotropic curvature flow in (1.3), we have a conservative geometric PDE as

$$\boldsymbol{n} \cdot \partial_t \boldsymbol{X} = -\mu, \qquad (4.1a)$$
$$\mu \boldsymbol{n} = -\partial_s(\boldsymbol{G}_k(\boldsymbol{n})\partial_s \boldsymbol{X}). \qquad (4.1b)$$

Suppose the initial curve $\boldsymbol{X}(\mathbb{T}, 0) = (x(\mathbb{T}, 0), y(\mathbb{T}, 0))^T := \Gamma_0 \in [H^1(\mathbb{T})]^2$ and the initial weighted curvature $\mu(\cdot, 0) := \mu_0(\cdot) \in H^1(\mathbb{T})$. Based on the conservative form (4.1), the variational formulation for anisotropic curvature flow is as follows: For any $t > 0$, find the solution $(\boldsymbol{X}(\cdot, t), \mu(\cdot, t)) \in [H^1(\mathbb{T})]^2 \times H^1(\mathbb{T})$ satisfying

$$\left(\boldsymbol{n} \cdot \partial_t \boldsymbol{X}, \varphi\right)_{\Gamma(t)} + \left(\mu, \varphi\right)_{\Gamma(t)} = 0, \qquad \forall \varphi \in H^1(\mathbb{T}), \qquad (4.2a)$$
$$\left(\mu \boldsymbol{n}, \boldsymbol{\omega}\right)_{\Gamma(t)} - \left(\boldsymbol{G}_k(\boldsymbol{n})\partial_s \boldsymbol{X}, \partial_s \boldsymbol{\omega}\right)_{\Gamma(t)} = 0, \quad \forall \boldsymbol{\omega} \in [H^1(\mathbb{T})]^2. \qquad (4.2b)$$

And the SP-PFEM for the anisotropic curvature flow (4.2) is as follows: Suppose the initial approximation $\Gamma^0 = \boldsymbol{X}^0(\mathbb{T}) \in [\mathbb{K}^h]^2$ is given by $\boldsymbol{X}^0(\rho_j) = \boldsymbol{X}_0(\rho_j), \forall 0 \leq j \leq N$, then for any $m = 0, 1, 2, \ldots$, find the solution $(\boldsymbol{X}^m(\cdot), \mu^m(\cdot)) \in [\mathbb{K}^h]^2 \times \mathbb{K}^h$, such that

$$\left(\boldsymbol{n}^{m+\frac{1}{2}} \cdot \frac{\boldsymbol{X}^{m+1} - \boldsymbol{X}^m}{\tau}, \varphi^h\right)_{\Gamma^m}^h + \left(\mu^{m+1}, \varphi^h\right)_{\Gamma^m}^h = 0, \quad \forall \varphi^h \in \mathbb{K}^h, \qquad (4.3a)$$
$$\left(\mu^{m+1}\boldsymbol{n}^{m+\frac{1}{2}}, \boldsymbol{\omega}^h\right)_{\Gamma^m}^h - \left(\boldsymbol{G}_k(\boldsymbol{n}^m)\partial_s \boldsymbol{X}^{m+1}, \partial_s \boldsymbol{\omega}^h\right)_{\Gamma^m}^h = 0, \quad \forall \boldsymbol{\omega}^h \in [\mathbb{K}^h]^2. \qquad (4.3b)$$

We refer $\boldsymbol{n}^{m+\frac{1}{2}}$ to (2.38)

For the SP-PFEM (4.3), we have

Theorem 4.1 *(Structure-preserving) Suppose $\gamma(\boldsymbol{n})$ satisfies (1.6) and take a stabilizing function $k(\boldsymbol{n}) \geq k_0(\boldsymbol{n})$, then the SP-PFEM (4.3) preserves area decay rate and energy dissipation, i.e.,*

$$\frac{A^{m+1} - A^m}{\tau} = -\left(\mu^{m+1}, 1\right)_{\Gamma^m}^h, \quad W^{m+1} \leq W^m \leq \ldots \leq W^0, \quad \forall m \geq 0. \quad (4.4)$$

Proof From [8, Theorem 2.1], we know that

$$A^{m+1} - A^m = \left(\boldsymbol{n}^{m+\frac{1}{2}} \cdot (\boldsymbol{X}^{m+1} - \boldsymbol{X}^m), 1\right)_{\Gamma^m}^h. \quad (4.5)$$

Thus, by taking $\varphi^h \equiv 1 \in \mathbb{K}^h$ in (4.3a), we obtain

$$\frac{A^{m+1} - A^m}{\tau} = \left(\boldsymbol{n}^{m+\frac{1}{2}} \cdot \frac{\boldsymbol{X}^{m+1} - \boldsymbol{X}^m}{\tau}, 1\right)_{\Gamma^m}^h = -\left(\mu^{m+1}, 1\right)_{\Gamma^m}^h, \quad (4.6)$$

which is the desired decay rate in (4.4).

For energy dissipation, we have already known that (3.16) is true. Taking $\varphi^h = \mu^{m+1}$ in (4.3a) and $\boldsymbol{\omega}^h = \boldsymbol{X}^{m+1} - \boldsymbol{X}^m$ in (4.3b), we know that

$$\begin{aligned}
0 &\geq -\tau\left(\mu^{m+1}, \mu^{m+1}\right)_{\Gamma^m}^h \\
&= \left(\boldsymbol{G}_k(\boldsymbol{n}^m)\partial_s \boldsymbol{X}^{m+1}, \partial_s(\boldsymbol{X}^{m+1} - \boldsymbol{X}^m)\right)_{\Gamma^m}^h \geq W^{m+1} - W^m,
\end{aligned}$$

which proves the claim. $\qquad\square$

Remark 4.1 It is worthwhile to compare our SP-PFEM (4.3) with the energy-stable PFEM for anisotropic curvature flow in [10] (often named the BGN scheme) proposed by Barrett, Garcke, and Nürnberg. The BGN scheme requires $\gamma(\boldsymbol{n})$ to be a special form $\gamma_{BGN}(\boldsymbol{n}) = \left(\sum_{l=1}^L \sqrt{(\boldsymbol{n}^T G_l \boldsymbol{n})^r}\right)^{\frac{1}{r}}$ with $\infty > r \geq 1$, $L \geq 1$ and $G_l \in \mathbb{R}^{2\times2}$ positive definite $\forall 1 \leq l \leq L$. Clearly, $\gamma_{BGN}(-\boldsymbol{n}) = \gamma_{BGN}(\boldsymbol{n}) < 3\gamma_{BGN}(\boldsymbol{n})$; thus, it satisfies the energy-stable condition (1.6). Therefore, our (4.3) can handle a broader range of anisotropies compared to the BGN scheme.

4.2 Area-conserved anisotropic curvature flow

Similarly, for the area-conserved anisotropic curvature flow in (1.3), the conservative geometric PDE is given as

$$\boldsymbol{n} \cdot \partial_t \boldsymbol{X} = -\mu + \lambda(t), \quad (4.7a)$$
$$\mu\boldsymbol{n} = -\partial_s(\boldsymbol{G}_k(\boldsymbol{n})\partial_s \boldsymbol{X}), \quad (4.7b)$$

where $\lambda(t)$ is given as (1.4) by replacing λ and Γ by $\lambda(t)$ and $\Gamma(t)$, respectively. And the variational formulation can be derived in a similar way.

In order to design a structure-preserving full discretization, we need to properly discretize $\lambda(t)$. Denote $\lambda^{m,*}$ with respect to Γ^m as

$$\lambda^{m,*} := \frac{\left(\mu^{m+1}, 1\right)_{\Gamma^m}^h}{(1, 1)_{\Gamma^m}^h}. \tag{4.8}$$

By adopting this $\lambda^{m,*}$, the SP-PFEM for the area-conserved anisotropic curvature flow in (1.3) is as follows: Suppose the initial approximation $\Gamma^0 = X^0(\mathbb{T}) \in [\mathbb{K}^h]^2$ is given by $X^0(\rho_j) = X_0(\rho_j), \forall 0 \leq j \leq N$; for any $m = 0, 1, 2, \ldots$, find the solution $(X^m(\cdot), \mu^m(\cdot)) \in [\mathbb{K}^h]^2 \times \mathbb{K}^h$, such that

$$\left(n^{m+\frac{1}{2}} \cdot \frac{X^{m+1} - X^m}{\tau}, \varphi^h\right)_{\Gamma^m}^h + \left(\mu^{m+1} - \lambda^{m,*}, \varphi^h\right)_{\Gamma^m}^h = 0, \quad \forall \varphi^h \in \mathbb{K}^h, \tag{4.9a}$$

$$\left(\mu^{m+1} n^{m+\frac{1}{2}}, \omega^h\right)_{\Gamma^m}^h - \left(G_k(n^m)\partial_s X^{m+1}, \partial_s \omega^h\right)_{\Gamma^m}^h = 0, \quad \forall \omega^h \in [\mathbb{K}^h]^2. \tag{4.9b}$$

For the above SP-PFEM (4.9), we have

Theorem 4.2 *(structure-preserving) Suppose $\gamma(n)$ satisfies (1.6) and take a finite stabilizing function $k(n) \geq k_0(n)$, then the SP-PFEM (4.3) is structure-preserving, i.e.,*

$$A^{m+1} \equiv A^0, \quad W^{m+1} \leq W^m \leq \ldots \leq W^0, \quad \forall m \geq 0. \tag{4.10}$$

Proof For the area conservation, taking $\varphi^h \equiv 1$ in (4.9a) yields that

$$\left(n^{m+\frac{1}{2}} \cdot (X^{m+1} - X^m), 1\right)_{\Gamma^m}^h = -\tau\left(\mu^{m+1} - \lambda^{m,*}, 1\right)_{\Gamma^m}^h$$

$$= -\tau\left(\mu^{m+1}, 1\right)_{\Gamma^m}^h + \tau \frac{\left(\mu^{m+1}, 1\right)_{\Gamma^m}^h}{(1, 1)_{\Gamma^m}^h}\left(1, 1\right)_{\Gamma^m}^h$$

$$= 0, \quad m \geq 0.$$

By noting (4.4), we deduce that $A^{m+1} - A^m = 0$, which shows area conservation (2.39a).

For energy dissipation, by the Cauchy inequality, we have

$$\left(\lambda^{m,*}, \mu^{m+1}\right)_{\Gamma^m}^h = \lambda^{m,*}\left(1, \mu^{m+1}\right)_{\Gamma^m}^h$$

$$= \frac{1}{(1, 1)_{\Gamma^m}^h}\left(\left(1, \mu^{m+1}\right)_{\Gamma^m}^h\right)^2$$

$$\leq \frac{1}{(1, 1)_{\Gamma^m}^h}\left(1, 1\right)_{\Gamma^m}^h\left(\mu^{m+1}, \mu^{m+1}\right)_{\Gamma^m}^h$$

$$= \left(\mu^{m+1}, \mu^{m+1}\right)_{\Gamma^m}^h, \quad m \geq 0.$$

Taking $\varphi^h = \mu^{m+1}$ in (4.9a) and $\boldsymbol{\omega}^h = \boldsymbol{X}^{m+1} - \boldsymbol{X}^m$ in (4.9b), and adopting the energy estimation (3.16) yields that

$$W^{m+1} - W^m \leq -\tau \left(\mu^{m+1} - \lambda^{m,*}, \mu^{m+1} \right)_{\Gamma^m}^h \leq 0, \qquad m \geq 0, \qquad (4.11)$$

which implies the energy dissipation in (4.10).   □

5 Numerical results

In this section, we present numerical experiments to illustrate the high performance of the proposed SP-PFEMs. The implementations and performances of the three SP-PFEMs are very similar. Thus in Sect. 5.1, we only show test results of the SP-PFEM (2.36) for the anisotropic surface diffusion. The morphological evolutions for three anisotropic geometric flows are shown in Sect. 5.2.

To compute the minimal stabilizing function $k_0(\boldsymbol{n})$, we first solve the optimization problem (2.41) for 20 uniformly distributed points $\boldsymbol{n}_j = (-\sin\frac{\pi}{10}j, \cos\frac{\pi}{10}j)^T \in \mathbb{S}^1$ to get $k_0(\boldsymbol{n}_j)$ for $j = 1, \ldots, 20$. Then for the general intermediate point $\boldsymbol{n} = (-\sin\theta, \cos\theta)^T \in \mathbb{S}^1$, say $\frac{\pi}{10}j < \theta < \frac{\pi}{10}(j+1)$, we do linear interpolation and set $k_0(\boldsymbol{n}) = \frac{10}{\pi}[(\theta - \frac{\pi}{10}j)k_0(\boldsymbol{n}_j) + (\frac{\pi}{10}(j+1) - \theta)k_0(\boldsymbol{n}_{j+1})]$. In Newton's iteration, the tolerance value ε is set as 10^{-12}.

5.1 Results for the anisotropic surface diffusion

Here we provide convergence tests to show the quadratic convergence rate in space and linear convergence rate in time. To this end, the time step τ is always chosen as $\tau = h^2$ except it is stated otherwise. The distance between two closed curves Γ_1, Γ_2 is given by the manifold distance $M(\Gamma_1, \Gamma_2)$ in [50] as

$$M(\Gamma_1, \Gamma_2) := 2|\Omega_1 \cup \Omega_2| - |\Omega_1| - |\Omega_2|, \qquad (5.1)$$
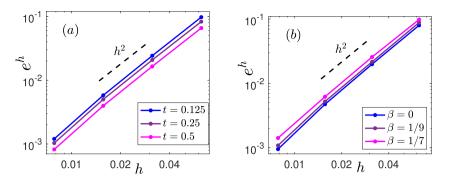
where Ω_1, Ω_2 are the interior regions of Γ_1, Γ_2, respectively, and $|\Omega|$ denotes the area of Ω. Let Γ^m be the numerical approximation of $\Gamma^h(t = t_m)$, $t_m := m\tau$ with mesh size h and time step τ, the numerical error is thus given as

$$e^h(t)\Big|_{t=t_m} := M(\Gamma^m, \Gamma(t_m)). \qquad (5.2)$$
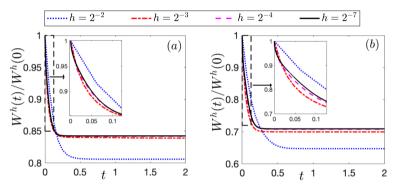
To numerically test the energy stability, area conservation and good mesh quality, we introduce the following indicators: the normalized energy $\frac{W^h(t)}{W^h(0)}\Big|_{t=t_m} := \frac{W^m}{W^0}$, the normalized area loss and the mesh ratio

$$\frac{\Delta A^h(t)}{A^h(0)}\Big|_{t=t_m} := \frac{A^m - A^0}{A^0}, \qquad R^h(t)\Big|_{t=t_m} := \frac{\max\limits_{1\leq j\leq N} |\boldsymbol{h}_j^m|}{\min\limits_{1\leq j\leq N} |\boldsymbol{h}_j^m|}. \qquad (5.3)$$

Fig. 2 Convergence rates of the SP-PFEM (2.36) with $k(\boldsymbol{n}) = k_0(\boldsymbol{n})$ for: **a** anisotropy in Case I at different times $t = 0.125, 0.25, 0.5$; and **b** anisotropy in Case II at time $t = 0.5$ with different β
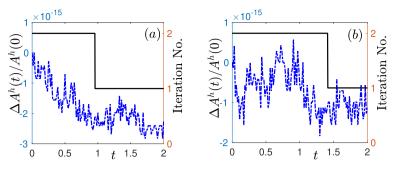

Fig. 3 Normalized energy of the SP-PFEM (2.36) with $k(\boldsymbol{n}) = k_0(\boldsymbol{n})$ and different h for: **a** anisotropy in Case I; **b** anisotropy in Case II with $\beta = \frac{1}{3}$

In the following numerical tests, the initial curve Γ_0 is given as an ellipse $\Gamma_0 = \{(2\cos\theta, \frac{1}{2}\sin\theta)^T, \forall 0 \le \theta < 2\pi\}$ with major axis 4 and minor axis 1. The exact solution $\Gamma(t)$ is approximated by choosing $k(\boldsymbol{n}) = k_0(\boldsymbol{n})$ with $h = 2^{-8}$ and $\tau = 2^{-16}$ in (2.36). Here are two typical anisotropic surface energies to be taken in our simulations:

- Case I: $\gamma(\boldsymbol{n}) = \sqrt{\left(\frac{5}{2} + \frac{3}{2}\mathrm{sgn}(n_1)\right)n_1^2 + n_2^2}$ [20];
- Case II: $\gamma(\boldsymbol{n}) = 1 + \beta\cos(3\theta)$ with $\boldsymbol{n} = (\sin\theta, -\cos\theta)^T$ and $|\beta| < 1$ [32]. It is weakly anisotropic when $|\beta| < \frac{1}{8}$, and otherwise it is strongly anisotropic.

Figure 2 presents the convergence rates of the proposed SP-PFEM (2.36) at different times and with different anisotropic strengths β for fixed time $t = 0.5$. It is apparent from this figure that the second-order convergence in space is independent of anisotropies and computation times, which indicates the convergence rate is very robust.

Fig. 4 Normalized area loss (blue dashed line) and iteration number (black line) of the SP-PFEM (2.36) with $k(\boldsymbol{n}) = k_0(\boldsymbol{n})$ and $h = 2^{-7}$, $\tau = h^2$ for: **a** anisotropy in Case I; **b** anisotropy in Case II with $\beta = \frac{1}{3}$
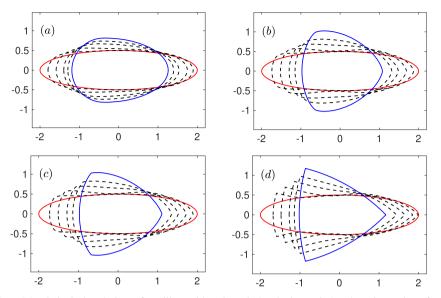

Fig. 5 Mesh ratio of the SP-PFEM (2.36) with $k(\boldsymbol{n}) = k_0(\boldsymbol{n})$ and different h for: **a** anisotropy in Case I; **b** anisotropy in Case II with $\beta = \frac{1}{3}$ (color figure online)

The time evolution of the normalized energy $\frac{W^h(t)}{W^h(0)}$ with different h, the normalized area loss $\frac{\Delta A^h(t)}{A^h(0)}$ and the number of Newton iterations with $h = 2^{-7}$, and the mesh ratio $R^h(t)$ with different h are summarised in Figs. 3, 4, 5, respectively.

It can be seen from Figs. 3, 4, 5 that

(i) The normalized energy is monotonically decreasing when the surface energy density satisfies the energy stable condition (1.6) (cf. Fig. 3);

(ii) The normalized area loss is at 10^{-15} which is almost in the same order as the round-off error (cf. Fig. 3), which confirms the area conservation in practical simulations;

(iii) Interestingly, the numbers of iterations in Newton's method are initially 2 and finally 1 (cf. Fig. 4). This finding suggests that although the proposed SP-PFEM (2.36) is full-implicit, but it can be solved very efficiently with a few iterations;

(iv) In Fig. 5 there is a clear trend of convergence of the mesh ratio R^h. Moreover, in contrast to the symmetrized SP-PFEM for symmetric $\gamma(\boldsymbol{n})$ in [4], R^h keeps small even with the strongly anisotropy $\gamma(\boldsymbol{n}) = 1 + \frac{1}{3}\cos 3\theta$.
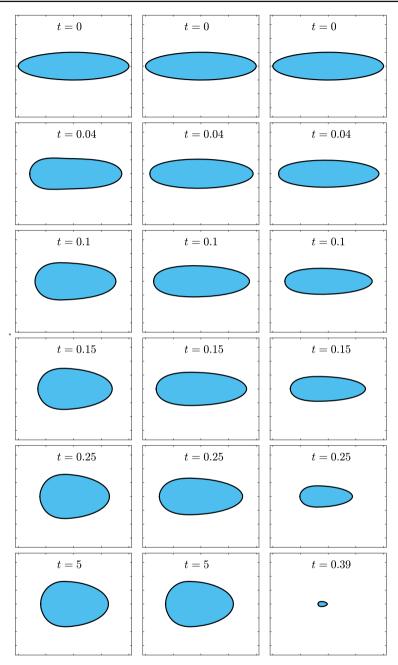
Fig. 6 Morphological evolutions of an ellipse with major axis 4 and minor axis 1 under anisotropic surface diffusion with four different anisotropic energies: **a** anisotropy in Case I; **b–d** anisotropies in case II with $\beta = 1/9, 1/7, 1/3$, respectively. The red and blue lines represent the initial curve and the numerical equilibrium, respectively; and the black dashed lines represent the intermediate curves. The mesh size and time step are taken as $h = 2^{-7}$, $\tau = h^2$ (color figure online)

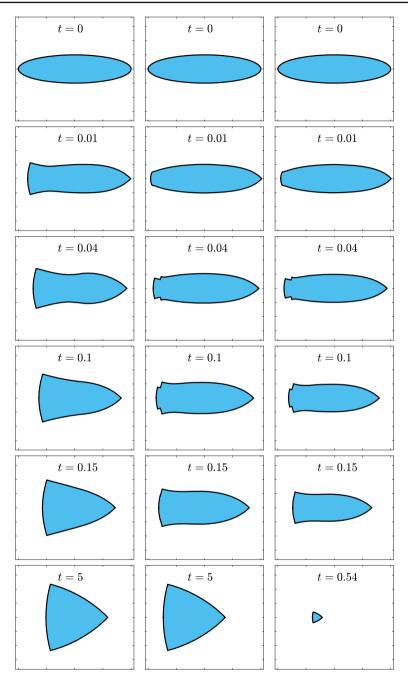### 5.2 Application for morphological evolutions

Finally, we apply the proposed SP-PFEMs to simulate the morphological evolutions of an ellipse with major axis 4 and minor axis 1 driven by the three anisotropic geometric flows. Figure 6 plots the morphological evolutions of anisotropic surface diffusion for the four different anisotropic energies: (a) anisotropy in case I; (b)–(d) anisotropies in case II with $\beta = 1/9, 1/7, 1/3$, respectively. Figures 7 and 8 depict the anisotropic surface diffusion, area-conserved anisotropic curvature flow, and anisotropic curvature flow at different times with anisotropy in case I and in case II with $\beta = 1/3$, respectively. Since anisotropic curvature flow will shrink to a point, we also illustrate its area $A^h(t)$ and its area decay rate in Fig. 9.

As shown in Fig. 6b–d, the edges emerge during the evolution and corners become sharper as the strength β increases. In fact, if the equilibrium is a polygon, $\gamma(\boldsymbol{n})$ is termed 'crystalline' [36]. While studies such as [4, 10, 38] mainly focus on the regularization of symmetric crystalline, our SP-PFEM (2.36) can also work for non-symmetric case.
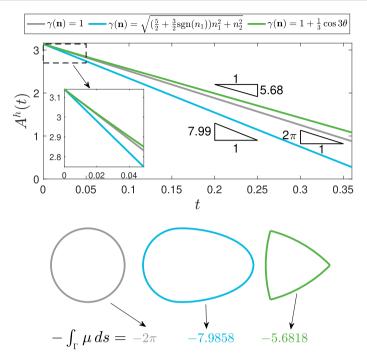
In contrast, from Fig. 6a, we observe that there are no edges or corners in the morphological evolutions with anisotropy in Case I. This suggests that even $\gamma(\boldsymbol{p}) = \sqrt{\left(\frac{5}{2} + \frac{3}{2}\mathrm{sgn}(p_1)\right)p_1^2 + p_2^2}$ is not a C^2-function, it is more like weak anisotropy! From Figs. 7, 8, we can see that the anisotropic surface diffusion and the area-conserved anisotropic curvature flow have the same equilibriums in shapes, while they have

Fig. 7 Morphological evolutions of an ellipse with major axis 4 and minor axis 1 under anisotropic surface diffusion (left column), area-conserved anisotropic curvature flow (middle column) and anisotropic curvature flow (right column) with the anisotropic surface energy density in Case I at different times. The evolving curves and their enclosed regions are colored blue and black. The mesh size and time step are taken as $h = 2^{-7}$, $\tau = 0.001$ (color figure online)

Fig. 8 Morphological evolutions of an ellipse with major axis 4 and minor axis 1 under anisotropic surface diffusion (left column), area-conserved anisotropic curvature flow (middle column) and anisotropic curvature flow (right column) with the anisotropic surface energy density in Case II with $\beta = 1/3$ at different times. The evolving curves and their enclosed regions are colored blue and black. The mesh size and time step are taken as $h = 2^{-7}$, $\tau = 0.001$

Fig. 9 Area and area decay rate of an ellipse with major axis 4 and minor axis 1 under anisotropic curvature flow by SP-PFEM (4.3) with different anisotropic energy densities: (i) $\gamma(\mathbf{n}) = 1$ (gray line); (ii) $\gamma(\mathbf{n}) = \sqrt{\left(\frac{5}{2} + \frac{3}{2}\text{sgn}(n_1)\right) n_1^2 + n_2^2}$ (blue line) and (iii) $\gamma(\mathbf{n}) = 1 + \frac{1}{3}\cos 3\theta$ (green line). The area decay rate is given by the chemical potential and the equilibrium. And the equilibriums are obtained from Fig. 6

different dynamics, i.e., the equilibriums are different in positions, and the anisotropic surface diffusion evolves faster than the area-conserved anisotropic curvature flow.

In isotropic curvature flow, the area decay rate $\frac{dA(t)}{dt} = -\int_{\Gamma} \kappa \, ds = -2\pi$ remains a constant during the whole process [14]. It is important to examine the impact of anisotropic effects on the area decay rate. As illustrated in Fig. 9, the area $A^h(t)$ exhibits a nearly linear decay rate for different anisotropies. However, the area decay rate does not remain at -2π. Instead, it approaches a different constant, $-\int_{\Gamma} \mu \, ds$, where Γ is the equilibrium state of the anisotropic surface diffusion (see Fig. 6). We also observe that the area decay rate may deviate from $-\int_{\Gamma} \mu \, ds$ at the beginning, presenting a remarkable contrast to the constant area decay rate of -2π in isotropic curvature flow.

6 Conclusions

By introducing a novel surface energy matrix $\mathbf{G}_k(\mathbf{n})$ depending on the anisotropic surface energy density $\gamma(\mathbf{n})$ and the Cahn-Hoffman $\boldsymbol{\xi}$-vector as well as a nonnegative stabilizing function $k(\mathbf{n})$, we proposed conservative geometric partial differential

equations for several geometric flows with anisotropic surface energy density $\gamma(\boldsymbol{n})$. We derived their weak formulations and applied PFEM to get their full discretizations. Subsequently, we proved these PFEMs are structure-preserving under a mild condition on $\gamma(\boldsymbol{n})$ with proper choice of the stabilizing function $k(\boldsymbol{n})$. Although our surface energy matrix $\boldsymbol{G}_k(\boldsymbol{n})$ is no longer symmetric, our experiments have shown it maintains a robust second-order convergence rate in space, a linear convergence rate in time, and unconditional energy stability. Specifically, the mesh quality of the proposed SP-PFEM, i.e. the mesh ratio is much smaller, is much better than that in the symmetrized SP-PFEM proposed recently for anisotropic surface diffusion with a symmetric surface energy density [4, 6]. Moreover, our SP-PFEMs work well for the piecewise C^2 anisotropy, which is a significant achievement compared with other PFEMs. In the future, we will generalize the surface energy matrix $\boldsymbol{G}_k(\boldsymbol{n})$ to three dimensions (3D) and propose efficient and accurate SP-PFEM for anisotropic geometric flows in 3D.

References

1. Andrews, B.: Volume-preserving anisotropic mean curvature flow. Indiana Univ. Math. J., 783-827 (2001)
2. Bao, W., Garcke, H., Nürnberg, R., Zhao, Q.: Volume-preserving parametric finite element methods for axisymmetric geometric evolution equations. J. Comput. Phys. **460**, 111180 (2022)
3. Bao, W., Garcke, H., Nürnberg, R., Zhao, Q.: A structure-preserving finite element approximation of surface diffusion for curve networks and surface clusters. Numer. Methods Partial Differ. Equ. **39**, 759–794 (2023)
4. Bao, W., Jiang, W., Li, Y.: A symmetrized parametric finite element method for anisotropic surface diffusion of closed curves. SIAM J. Numer. Anal. **61**(2), 617–641 (2023)
5. Bao, W., Jiang, W., Wang, Y., Zhao, Q.: A parametric finite element method for solid-state dewetting problems with anisotropic surface energies. J. Comput. Phys. **330**, 380–400 (2017)
6. Bao, W., Li, Y.: A symmetrized parametric finite element method for anisotropic surface diffusion in three dimensions. SIAM J. Sci. Comput. **45**(4), A1438–A1461 (2023)
7. Bao, W., Zhao, Q.: An energy-stable parametric finite element method for simulating solid-state dewetting problems in three dimensions. J. Comput. Math. **41**, 771–796 (2023)
8. Bao, W., Zhao, Q.: A structure-preserving parametric finite element method for surface diffusion. SIAM J. Numer. Anal. **59**(5), 2775–2799 (2021)
9. Barrett, J.W., Garcke, H., Nürnberg, R.: A parametric finite element method for fourth order geometric evolution equations. J. Comput. Phys. **222**(1), 441–467 (2007)
10. Barrett, J.W., Garcke, H., Nürnberg, R.: Numerical approximation of anisotropic geometric evolution equations in the plane. IMA J. Numer. Anal. **28**(2), 292–330 (2008)
11. Barrett, J.W., Garcke, H., Nürnberg, R.: On the parametric finite element approximation of evolving hypersurfaces in $\mathbb{R}^3$. J. Comput. Phys. **227**(9), 4281–4307 (2008)
12. Barrett, J.W., Garcke, H., Nürnberg, R.: A variational formulation of anisotropic geometric evolution equations in higher dimensions. Numer. Math. **109**(1), 1–44 (2008)
13. Barrett, J.W., Garcke, H., Nürnberg, R.: Finite-element approximation of coupled surface and grain boundary motion with applications to thermal grooving and sintering. Eur. J. Appl. Math. **21**(6), 519–556 (2010)
14. Barrett, J.W., Garcke, H., Nürnberg, R.: Parametric finite element approximations of curvature-driven interface evolutions. Handb. Numer. Anal. **21**, 275–423 (2020)

15. Cahn, J.: Stability, microstructural evolution, grain growth, and coarsening in a two-dimensional two-phase microstructure. Acta Metall. Mater. **39**(10), 2189–2199 (1991)
16. Cahn, J.W., Taylor, J.E.: Overview no. 113 surface motion by surface diffusion. Acta Metall. Mater. **42**(4), 1045–1063 (1994)
17. Carter, W.C., Roosen, A., Cahn, J.W., Taylor, J.E.: Shape evolution by surface diffusion and surface attachment limited kinetics on completely faceted surfaces. Acta Metall. Mater. **43**(12), 4309–4323 (1995)
18. Chen, Y., Giga, Y., Goto, S.: Uniqueness and existence of viscosity solutions of generalized mean curvature flow equations. In: Fundamental Contributions to the Continuum Theory of Evolving Phase Interfaces in Solids, pp. 375–412. Springer, Berlin (1999)
19. Clarenz, U., Diewald, U.,Rumpf, M.: Anisotropic geometric diffusion in surface processing. IEEE Vis. (2000)
20. Deckelnick, K., Dziuk, G., Elliott, C.M.: Computation of geometric partial differential equations and mean curvature flow. Acta Numer. **14**, 139–232 (2005)
21. Deckelnick, K., Dziuk, G., Elliott, C.M.: Fully discrete finite element approximation for anisotropic surface diffusion of graphs. SIAM J. Numer. Anal. **43**(3), 1112–1138 (2005)
22. Dolcetta, I.C., Vita, S.F., March, R.: Area-preserving curve-shortening flows: from phase separation to image processing. Interfaces Free Bound. **4**(4), 325–343 (2002)
23. Du, P., Khenner, M., Wong, H.: A tangent-plane marker-particle method for the computation of three-dimensional solid surfaces evolving by surface diffusion on a substrate. J. Comput. Phys. **229**(3), 813–827 (2010)
24. Du, Q., Feng, X.: The phase field method for geometric moving interfaces and their numerical approximations. Handb. Numer. Anal **21**, 425–508 (2020)
25. Dziuk, G.: An algorithm for evolutionary surfaces. Numer. Math. **58**(1), 603–611 (1990)
26. Dziuk, G.: Convergence of a semi-discrete scheme for the curve shortening flow. Math. Models Methods Appl. Sci. **04**(4), 589–606 (1994)
27. Fonseca, I., Pratelli, A., Zwicknagl, B.: Shapes of epitaxially grown quantum dots. Arch. Ration. Mech. Anal. **214**, 359–401 (2014)
28. Girao, P.M., Kohn, R.V.: The crystalline algorithm for computing motion by curvature. In: Variational Methods for Discontinuous Structures, pp. 7–18. Springer, Berlin (1996)
29. Gurtin, M.E., Jabbour, M.E.: Interface evolution in three dimensions with curvature-dependent energy and surface diffusion: interface-controlled evolution, phase transitions, epitaxial growth of elastic films. Arch. Ration. Mech. Anal. **163**, 171–208 (2002)
30. Hoffman, D.W., Cahn, J.W.: A vector thermodynamics for anisotropic surfaces: I. Fundamentals and application to plane surface junctions. Surf. Sci. **31**, 368–388 (1972)
31. Jiang, W., Bao, W., Thompson, C.V., Srolovitz, D.J.: Phase field approach for simulating solid-state dewetting problems. Acta Mater. **60**(15), 5578–5592 (2012)
32. Jiang, W., Wang, Y., Zhao, Q., Srolovitz, D.J., Bao, W.: Solid-state dewetting and island morphologies in strongly anisotropic materials. Scr. Mater. **115**, 123–127 (2016)
33. Jiang, W., Zhao, Q.: Sharp-interface approach for simulating solid-state dewetting in two dimensions: A Cahn-Hoffman $\boldsymbol{\xi}$-vector formulation. Phys. D **390**, 69–83 (2019)
34. Kovács, B., Li, B., Lubich, C.: A convergent evolving finite element algorithm for mean curvature flow of closed surfaces. Numer. Math. **143**, 797–853 (2019)
35. Li, Y., Bao, W.: An energy-stable parametric finite element method for anisotropic surface diffusion. J. Comput. Phys. **446**, 110658 (2021)
36. Mercier, G., Novaga, M., Pozzi, P.: Anisotropic curvature flow of immersed curves. Commun. Anal. Geom. **27**(4), 937–964 (2019)
37. Niessen, W.J., Romeny, B.M., Florack, L.M., Viergever, M.A.: A general framework for geometry-driven evolution equations. Int. J. Comput. Vis. **21**(3), 187–205 (1997)
38. Perl, R., Pozzi, P., Rumpf, M.: A Nested Variational Time Discretization for Parametric Anisotropic Willmore Flow, pp. 221–241. Springer International Publishing, Berlin (2014)
39. Randolph, S., Fowlkes, J., Melechko, A., Klein, K., Meyer, I., Simpson, M., Rack, P.: Controlling thin film structure for the dewetting of catalyst nanoparticle arrays for subsequent carbon nanofiber growth. Nanotech. **18**(46), 465354 (2007)
40. Shen, H., Nutt, S., Hull, D.: Direct observation and measurement of fiber architecture in short fiber-polymer composite foam through micro-CT imaging. Compos. Sci. Technol. **64**(13–14), 2113–2120 (2004)

41. Sutton, A.P., Balluffi, R.W.: Interfaces in Crystalline Materials. Clarendon Press, Oxford (1995)
42. Taylor, J.E.: Mean curvature and weighted mean curvature. Acta Metall. Mater. **40**, 1475–1485 (1992)
43. Taylor, J.E., Cahn, J.W., Handwerker, C.A.: Overview no. 98 i–geometric models of crystal growth. Acta Metall. Mater. **40**(7), 1443–1474 (1992)
44. Thompson, C.V.: Solid-state dewetting of thin films. Annu. Rev. Mater. Res. **42**, 399–434 (2012)
45. Wang, Y., Jiang, W., Bao, W., Srolovitz, D.J.: Sharp interface model for solid-state dewetting problems with weakly anisotropic surface energies. Phys. Rev. B **91**(4), 045303 (2015)
46. Wheeler, A.: Cahn-Hoffman $\boldsymbol{\xi}$-vector and its relation to diffuse interface models of phase transitions. J. Stat. Phys. **95**, 1245–1280 (1999)
47. Wong, H., Voorhees, P., Miksis, M., Davis, S.: Periodic mass shedding of a retracting solid film step. Acta Mater. **48**(8), 1719–1728 (2000)
48. Xu, Y., Shu, C.: Local discontinuous Galerkin method for surface diffusion and Willmore flow of graphs. J. Sci. Comput. **40**(1–3), 375–390 (2009)
49. Ye, J., Thompson, C.V.: Mechanisms of complex morphological evolution during solid-state dewetting of single-crystal nickel thin films. Appl. Phys. Lett. **97**(7), 071904 (2010)
50. Zhao, Q., Jiang, W., Bao, W.: An energy-stable parametric finite element method for simulating solid-state dewetting. IMA J. Numer. Anal. **41**(3), 2026–2055 (2021)